Karlsruher Institut für Technologie

Light Technology Institute (LTI)
Engesserstraße 13
76131 Karlsruhe

Master Thesis

Design and construction of a light source setup for stray light measurements in array spectrometers

submitted by
Malte Kretz

January 16, 2018

Referent: Prof. Dr. rer. nat. Uli Lemmer
Supervisor: Dr. Johannes Brachmann

Erklärung

Ich versichere hiermit, dass ich meine Masterarbeit selbständig und unter Beachtung der Regeln zur Sicherung guter wissenschaftlicher Praxis im Karlsruher Institut für Technologie (KIT) in der aktuellen Fassung angefertigt habe. Ich habe keine anderen als die angegebenen Quellen und Hilfsmittel benutzt und wörtlich oder inhaltlich übernommene Stellen als solche kenntlich gemacht.

Karlsruhe, 15. Januar 2018

Malte Kretz

I would like to say thank you to everyone who motivated me and offered their support during the making of this thesis.

In the first place, I would like to thank Prof. Dr. rer. nat. Uli Lemmer who supervised and examined my master thesis.

Cordial thanks go out to Dr. Johannes Brachmann who lent me his support with a lot of patience, interest and cooperativeness. Thank you, too, for the very helpful suggestions and the constructive criticism during the production of this thesis.

I would also like to thank Dr. Peter Haschberger and everyone else at the DLR in Weßling for many interesting ideas and discussions which contributed to the fact that this thesis is what it is now.

Thank you to my girlfriend Daniela who behaved supportively towards me over the last months and was a tower during my master programme.

Last, but not least, a huge thank you goes to my family, who rendered my studies at the Karlsruhe Institute of Technology possible by their tremendous support and were always there for me with a friendly ear.

Contents

1 Introduction

The climate change caused by global warming is affecting the environment. To be able to monitor and document those changes the EnMAP satellite was devised. The EnMAP is equipped with an hyperspectral imaging spectrometer which records the reflected sunlight from the earth. The imaging spectrometer records a continuous spectrum for every pixel, which allows to directly identify and quantify the recorded materials. This enables, for example, to determine the type and condition of vegetation or identify substances in water.[7]

To be able to correctly associate the different reflectance spectra recorded to the corresponding materials, the data measured by the spectrometer is the key. As every practical spectrometer, the EnMAP spectrometer is affected by stray light. Stray light is caused, for example, by imperfections in the surfaces of its mirrors or chromatic aberrations of the used lenses and many more. This causes errors in the recorded data. However the stray light caused by the instrument is unique to it and can therefore be further characterized.

In order to characterize and correct the stray light in an instrument, different methods have been developed and reported [13] [20] [2]. One method is to light the instrument with spatially small, spectrally narrow, near monochromatic and high powered light. The goal is to illuminate only a small area of the detector [13]. The detectors response to that light allows to characterize the stray light originating from the instrument. This needs to be done for multiple wavelengths.

The goal of this thesis is to design, build and characterize such a light source. In the first chapter of this thesis the fundamentals behind such a setup will be discussed, starting with basic properties of light and its generation; then explaining the different causes of stray light in optical instruments and the methods to correct it. From there the theoretical boundaries for the design of such a light source will be elaborated. And finally presenting the measurement devices used for the characterization.

In the second chapter the light source setup and the methods used for its characterization will be explained. Commencing by, introducing in the first part, the light source setup and its technical realization. From thereon the experimental procedure for the characterization measurements of the EQ-99XFC light, the interference filters, their angular tuning and finally their optical density will be presented.

The third chapter will discuss the results of the characterization measurements presented above in the same order, starting with EQ-99XFC and from there going over to the filters.

Finally a conclusion from the measurements will be drawn and an outlook will be provided.

2 Fundamentals

2.1 Light generation

A simplified explanation for the generation of light can be given by using the Bohr model [16]. It depicts the structure of an atom by a positively charged nucleus which is surrounded by electrons. The electrons surround the nucleus in concentric, circular orbits. Each orbit represents an element specific energy level. In thermodynamic equilibrium, lower energy levels contain more electrons than higher ones [8]. This is described in the Boltzmann distribution, which is given by:

$$N_x = N_0 \cdot e^{-\frac{E_x}{k_B * T}} \tag{2.1}$$

N_x and N_0 represent the number of electrons in energy level x and 0, E the energy of state, k_B the Boltzmann constant and T the temperature of the system [18].

2.1.1 Spontaneous emission

Light is generated as a follow-up after the system described above is disrupted by an external addition of energy. The energy absorbed leads to an electron going to a higher energy state E_1. The excited electron may spontaneously decay back to a lower energy state E_0, the energy difference between them will be released in form of a photon. The process is depicted in figure 2.1.

$$E_{photon} = \Delta E = E_1 - E_0 \tag{2.2}$$

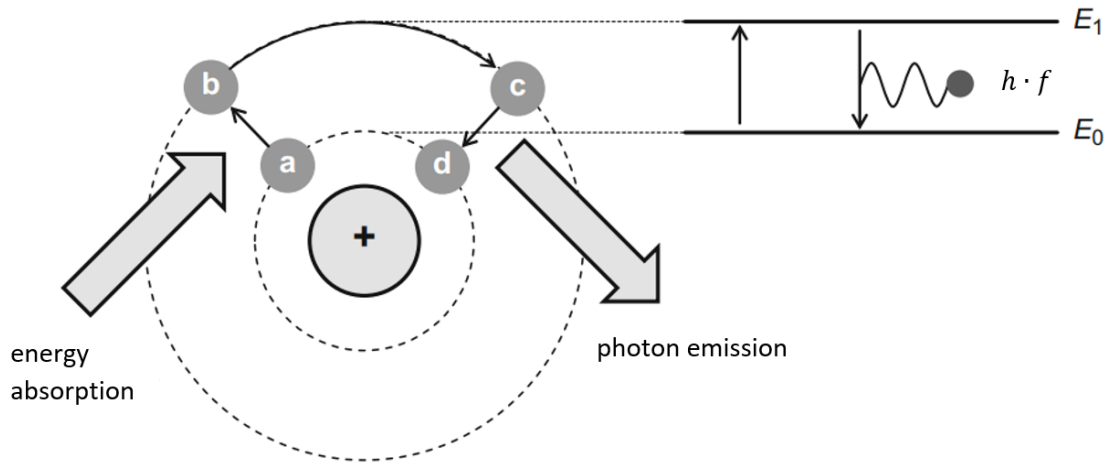

Figure 2.1: Process of spontaneous emission. Addition of energy to the system (a) which leads to an electron changing to a state of higher energy (b). Relaxation of the excited electron leads to photon emission (c) and for the electron to fall back into the lower Energy state(d). Taken from [8].

The resulting photon propagates like a wave. The Wave-particle duality of light originates from this.

The photon energy can also be described by the following equation:

$$E_{photon} = h \cdot f \tag{2.3}$$

Where h stands for the Planck constant and f for the frequency of the light. The frequency is the product of the speed of light in a vacuum c_0 and the wavelength λ. The wavelength is therefore the result of the Energy difference ΔE from equation 2.2.

$$f = \frac{c_0}{\lambda} \Leftrightarrow \lambda = \frac{c_0 \cdot h}{E_1 - E_0} \tag{2.4}$$

The description given doesn't account for non radiative recombination which can also occur.

2.1.2 Natural broadening

According to equation 2.4 each photon emitted should have a discrete wavelength. Those wavelengths are called lines. However, in reality radiation, has a specific width attributed to it. This width can be described by a gauss profile.

This is caused by the fact that an electron can only remain in its excited state for the time τ. Therefore, due to Heisenberg's uncertainty principle, the exact energy of the photon cannot be determined. From this results an energy uncertainty which leads to a spectral broadening of the light.

2.2 Light as a wave

Multiple observed light properties can be explained by considering that light propagates as an electromagnetic wave [5]. Notable examples of these are reflection, interference and diffraction of light. The properties of the electromagnetic wave can be described by using the Maxwell equations.

The electrical and magnetic field of a light wave are orthogonal to each other and transversal to its propagation direction. With the electrical field usually being stronger than the magnetic field, it is used to characterize the light wave. The covered distance during one oscillation describes the wavelength λ.

2.2.1 Geometrical optics

To understand light propagation on a macroscopic scale it can be described as rays. This level of abstraction allows to approximate the path the light is going to take under certain circumstances. For this, a number of assumptions need to be made. First that

in homogeneous materials light rays move straight. If the light ray hits the frontier between two materials with different refraction indexes the ray is reflected according to the laws of reflection and broken according to Snell's law. Furthermore the light path is reversible and finally that crossing light rays don't interfere with each other[10] [9].

2.3 Stray light in array spectrometers

A typical array spectrometer is made of an input optic, an entrance slit, a dispersing element and a detector array. Light coupled into it passes the input optic and goes through the entrance slit. From which it is pointed at the dispersing element (usually a grating or a prism). The setup described above is depicted in figure 2.2 The dispersing element causes the spatial image of the entrance slit to fall on different locations on the detector array, depending on its wavelength.

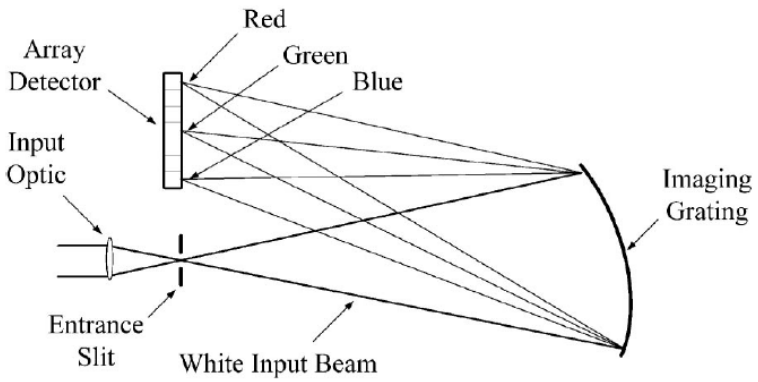

Figure 2.2: Illustration of an array spectrometer composed of a fixed imaging grating and a fixed multipixel array detector. Taken from [20].

In an ideal setup the light falling onto a specific detector element of the array is composed only of the corresponding spectral components of the light source. A typical detector array is depicted in figure 2.3. In practical setups however this is not the case. Surface imperfections of the dispersing elements lead to scattering of the incident light. Multiple reflections between the optical elements of the setup also cause scattering [20]. This misdirected light falls onto other detector elements and falsifies the image of the input light onto the detector. This is depicted in figure 2.3. This leads to lower contrast, reduced detail and color inaccuracy of the measurements [2]. That misdirected light is called stray light.

In order to diminish the effects of stray light onto the measurements of a certain instrument, the flaws in its image forming properties need to be determined. These flaws are described by the instruments stray light point-spread function (PSF) [12]. The PSF of a system can determined by theoretical analysis or via experimental procedures.

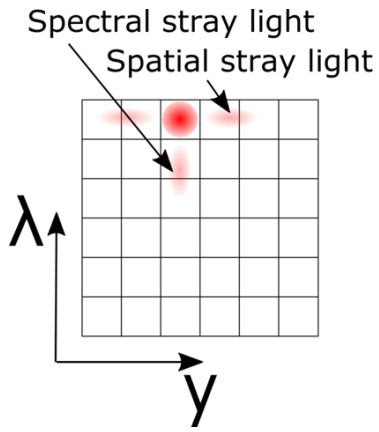

Figure 2.3: Illustration of spatial and spectral stray light on a detector array.

In order to determine the PSF experimentally a spectrally narrow and highly localized light source is needed. From the image of this light source produced by the imaging optics of the instrument onto its detector the PSF can be derived [4]. Because only small amounts of the incident light are misdirected, the light source used must be very powerful. This however causes saturation of the detector, which prevents the measurements in that region. Because the scattering effects are also wavelength dependent, in order to characterize them completely, the whole spectral range of the detector needs to be measured. An example for a PSF is depicted in figure 2.4. As stated above a high powered localized light source with a wavelength of 679 nm was used, from which the corresponding PSF depicted in figure 2.4 was derived.

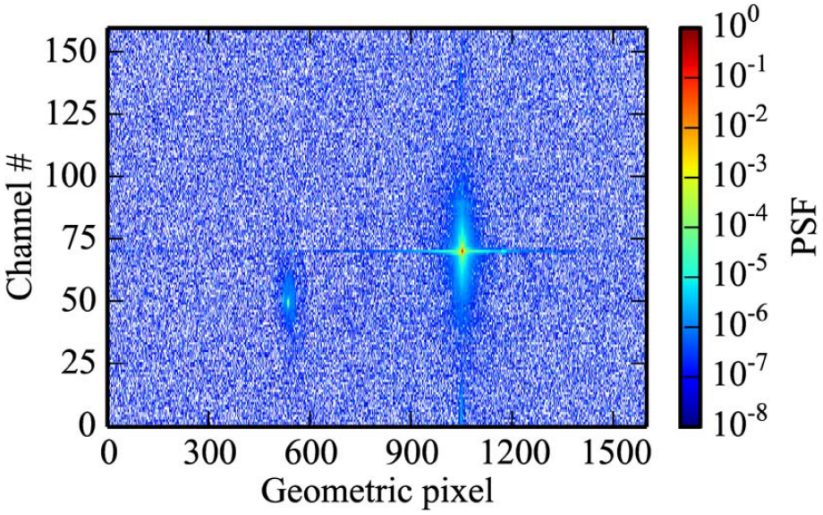

Figure 2.4: Image of a measured PSF, taken from [13].

2.3.1 Boundary conditions for the characterized light source

In order to build a measurement setup capable of measuring the effects of stray light in an instrument, certain conditions need to be met. These can be derived from section 2.3. The setup needs to be able to output light over the whole span of the instruments spectral range. For the EnMAP instrument the spectral range covers the VNIR and parts of the SWIR (420 nm to 2450 nm). The output light needs to be spectrally narrow, near monochromatic in order to reference the effects to a specific wavelength. Furthermore the output area of the light needs to be in the scale of the detector pixels, this is provided by an optical fiber. Which also allows the setup to be connected to a collimating device. The output optical power of the setup needs to be stable over the duration of the stray light measurements. The optical power of the light source is dependent on the characterized instrument and needs to be variable. On one hand it needs to be at 80% of the saturation level of the lit detector pixels and on the other hand it needs to high enough to oversaturate the pixels in the point of focus [13] . For the EnMAP instrument in high gain mode for example an optical power of 200 μW is needed which corresponds to a radiance in an order of magnitude around 600 $mW/cm^2/\mu m/sr$ for the VNIR part of its spectrum [7]. To meet these conditions the light generation in the setup is crucial. The different methods possible will be discussed in section 3.1.1.

2.3.2 Optical fibers

To guide light in an efficient matter, optical fibers were used during this thesis. This section discusses their basic properties. From those, arise certain possibilities and limitations which will also be discussed.

A typical optical fiber consists of two coaxial layers, usually in cylindrical form. The smaller cylinder is called the core whereas the surrounding part is called cladding. The cladding usually has a smaller refractive index than the core. Therefore, due to Snell's Law, light that enters the core is reflected from the cladding and stays in the core. The maximum angle for the total reflection also defines the angle for which incident light can be coupled into the core of the fiber. This angle θ is described by the Numerical Aperture NA of the fiber formulated in equation 2.5, n_i denotes the index of refraction of the outside material.

$$NA = n_i \cdot sin(\theta) \tag{2.5}$$

The light propagation in the fiber can be described with its properties. Due to the electromagnetic wave properties of light, only certain modes, depending on the core size can propagate in the core. Those must satisfy the electric and magnetic field boundary conditions in the core-cladding interface.

Fibers are classified depending on the number of modes they can propagate: Single Mode fibers(SMFs) and multimode fibers (MMFs). As the name implies SMF only propagate a single mode whereas MMF can guide multiple modes. Furthermore, the different fibers are separated into step-index and graded-index fibers. A step-

index fiber has a constant refractive index in the core and cladding material which leads to a drastic change at the core cladding boundary. A Graded-Index fiber has a refractive index which decreases gradually with the distance to the core center.

Optical fibers are often comprised of silica because of its good optical transmission characteristics.

2.3.3 Interference filters

An interference filter is an optical filter that reflects multiple different spectral bands and only transmits a specific band around a certain wavelength. This is achieved by a number of dielectric layers with alternating low and high refractive indices. Due to interference between incident and reflected waves in between the thin films the filter becomes highly wavelength selective [14]. The layers in such a filter are optimized for normal incidence.

If the incident light however isn't normal to the filter its central wavelength shifts. This is caused by a changing phase difference between the reflected and incident waves [15]. This phase difference results in a shift of the central wavelength to lower wavelengths. The relation between incident angle θ and resulting central wavelength λ is given by equation 2.6.

$$\lambda = \lambda_{max}\sqrt{1 - \frac{sin^2\theta}{n_{eff}^2}} \tag{2.6}$$

λ_{max} corresponds to the central wavelength at normal incidence $\theta = 0°$ and its index of refraction n_{eff} according to [1].

2.4 Measurement equipment

During the course of this thesis different measurement devices were used. This section will present them, first the used spectrometers and then the optical power meter. Two different optical spectrum analyzers from Yokogawa, a MCS 100 spectrometer from Zeiss and a the HR-1024i from the spectra vision company were used as spectrometers and will be presented in this order. Afterwards the Newport Power meter will be described.

2.4.1 Optical Spectrum Analyser (OSA)

An optical spectrum analyzer is different from a typical spectrometer. In contrast to grating spectrometers an OSA uses a Czerny-Turner monochromator [3]. In such a setup the light source goes through an entrance slit and is then collimated. The collimated beam is then reflected onto a optical grating. Due to diffraction on the grating the collimated light is dispersed. A second mirror is used to focus the light coming from the grating onto an exit slit (with the same size as the entrance slit) in front of the photo detector. Because of the dispersion the different wavelengths are spread out over the exit slit and

therefore only a specific part of the light spectra entering the instrument reaches the photo detector. The spectral resolution of this signal is dependent on the size of the slits.

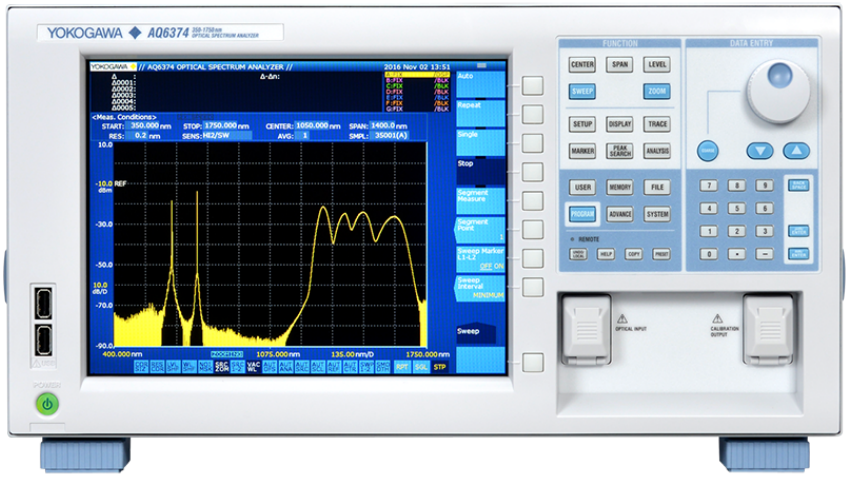

Figure 2.5: Image of an AQ6474, taken from the Yokogawa website.

An OSA therefore allows to measure the relative spectrum of a light source with a spectral resolution reaching up to 50 pm. Which, for example, can be used to accurately measure the slope of a transmission filters band edge.

The OSAs used in this thesis were the AQ6374 and the AQ6376 from Yokogawa, depicted in figure 2.5. The main difference between both of them lies in their wavelength range. The AQ6374 ranges from 350 nm to 1750 nm whereas the AQ6376 ranges from 1500 nm to 3400 nm. Both have an FC optical fiber connector as input. Due to different detectors in the devices their sensitivity is also diverging. The AQ6374 is able to detect signals up to -80 dBm whereas the AQ6376 is limited to -65 dBm. Their resolutions also diverge with AQ6374 being more precise with 0.05 nm in contrast to 0.1 nm. The specifications of the instruments were taken from the manufacturer data sheet [19].

2.4.2 Zeiss MCS 100 Spectrometer

The Zeiss MCS 100 spectrometer has spectral range from 600 nm to 1100 nm. Light is coupled into it via an optical fiber with SMA connector.

2.4.3 SVC HR-1024i

The SVC HR-1024i from the Spectra Vision company is a spectroradiometer, it is depicted in figure 2.6. With three different detectors it provides a spectral range starting from 350 nm to 2500 nm. Therefore it's ideal for the measurement of spectrally broad light sources such as the ones used in this thesis. Light can be coupled into it by using different input optics. An optical fiber, a lens or an integration sphere can be used. The SVC HR-1024i internal calibration was used for the measurements.

Figure 2.6: Image of the SVC HR-1024i with a lens optic input.

2.4.4 Newport Optical power meter

This section presents the Newport 1936-R optical power meter used during this thesis.

The 1936-R is designed to measure the optical power of monochromatic or near-monochromatic light sources. For this purpose the power meter comes with an input compatible with different photo detectors. The photo detectors convert the incoming light into electrical signals. With the device internal calibration a power value is attributed to the electrical signal. The 1936-R with two different detectors is depicted in figure 2.7. During this thesis the 1936-R was used together with the 918D-SL-OD3R detector, which has a spectral range from 400 nm to 1100 nm.

Figure 2.7: Image of the Newport 1936-R optical power meter with two different optical detectors, taken from the Newport website.

3 Experimental Procedure

This chapter will discuss the development and assembly of the light source setup and afterwards the experimental procedure for its characterization.

3.1 Building the light source setup

This section will explain how the light source setup described in section 2.3.1 is designed and which elements were selected to built it.

3.1.1 Light generation for the setup

To meet the conditions stated in section 2.3.1 three different approaches for light generation were considered. An LED based light source, a plasma light source and a laser based light source. The strength and weaknesses of the different systems will be discussed below.

One possibility was to use an LED based light source. Multiple LEDs would be used with each representing a specific band in the spectrum defined above. LEDs with optical powers of over 1000 mW can be purchased from specialized manufactures such as Thorlabs. However for each band of the light source a new LED needs to be integrated into the setup. With each individual LED requiring an adequate electrical driver. Furthermore the optical power output LEDs is temperature dependent and their aging processes need to be considered as well. With those factors being individual to each LED, this requires a high amount of work for each one. Therefore LEDs seemed not appropriate for the setup.

Tunable laser light sources such as the Fianium Whitelase or an opitcal parametric oscillators provide the required high radiances over the defined spectrum of 400 nm to 2500 nm. With a spectral power density of at least 2 mW/nm in the VNIR. However these light sources are pulsed and not continuous. The high peak optical power at the start of a pulse can damage the lit instrument. With this risk in mind these light sources were discarded as base for the setup.

The third possibility was the Xenon based plasma lamp EQ-99XFC from Energetiq. The lamp offers stable, high optical power over the required spectrum. In contrast to the other approaches the EQ-99XFC emits a continuous spectrum. Therefore it needs to be filtered in order to be used in the light source setup. This offers a high amount of flexibility since, in order to get a the necessary band, only a corresponding filter needs to be selected. The output is an optical fiber. Dependent on the core diameter of the output fiber the radiance required is provided. According to Energetiq the highest radiance is achieved using a 200 μm fiber due to the fact that the light emitting part of the plasma has a similar size. Furthermore with a life time exceeding 10000 h it's suited for long automated measurements. The required informations were taken from the manufactures data sheet [6]. The EQ-99XFC is depicted in figure 4.1

Figure 3.1: EQ-99XFC plasma light source with pumping laser, taken from the Energetiq website.

From the three possibilities presented above the plasma lamp meets the necessary requirements the best. Therefore it will serve as light generation device for the light source setup.

3.1.2 Schematic setup

The base of the light source setup is the EQ-99XFC, as discussed above. For it, a theoretical setup was devised, which is depicted in figure 3.2. The setup transforms the broad emission spectrum of the EQ-99XFC at the input to the required narrow bands, referenced in section 2.3.1, at the output. The ideas behind the setup will be discussed below.

The EQ-99XFC emits a broad spectrum ranging from the deep UV with 120 nm up to 2700 nm. It therefore needs to be filtered in order to get spectrally narrow bands at the output of the setup. The quality of the used filters determines the quality of the final output. In order to be filtered the emitted light of the EQ-99XFC needs to be guided through the filters. This is achieved by collimating the light coming out of its output fiber. The collimated beam then passes the filters. The different filters need to be interchangeable automatically, without manual changes. After passing them, the beam is then coupled back into an optical fiber with the same core size as the EQ-99XFC in order to preserve its radiance. To get a power monitoring that is mechanically independent from the filtering part of the setup a second free ray part is integrated into the setup. The light is once again collimated after which the beam is split. One part is guided upon a photon detecting device for control measurement purposes whereas the other part passes a shutter which can set the output of the setup on and off. Afterwards it is coupled into an output fiber with a rectangular core.

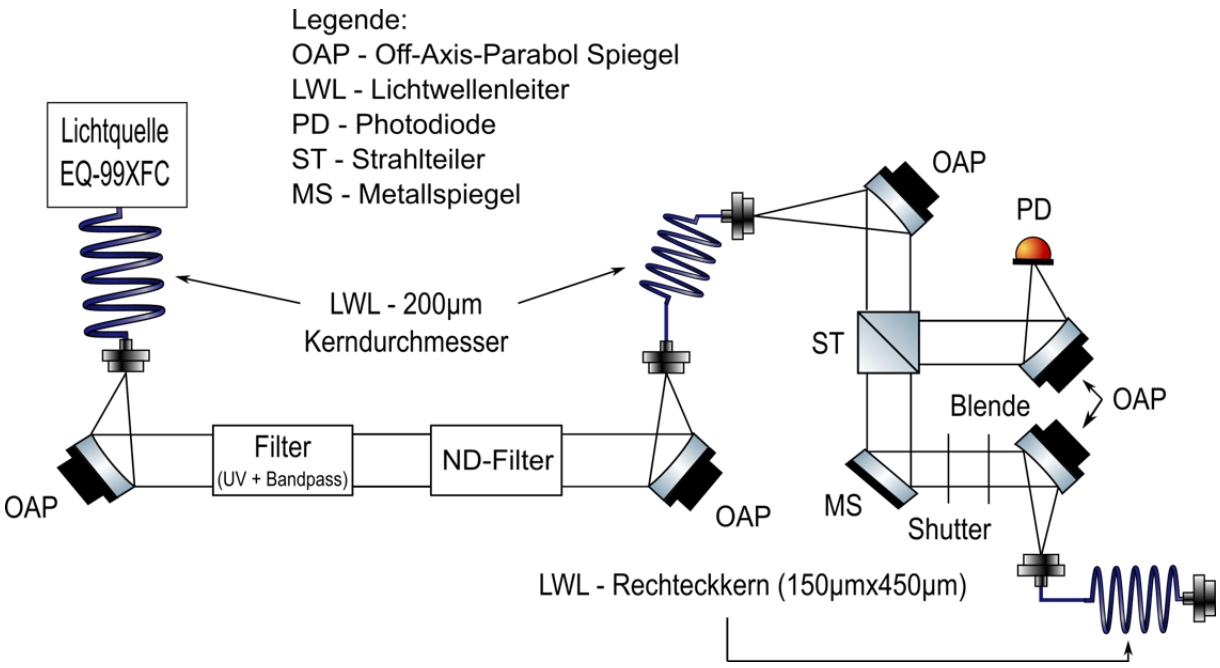

Figure 3.2: Sketch of the light source setup.

The choice of the specific parts for the described setup will be discussed in the next section.

3.1.3 Technical realization

This section discusses the technical realization of the setup described previously. Starting with the used filters and their integration into the setup, going over to the collimation of the light emitted by the EQ-99XFC, which leads to methods to align the light in the setup.

The backbone for the light source setup are the used filters and the EQ-99XFC. Since the properties of the EQ-99XFC were already discussed in section 3.1.1, the filters used in the setup need to be chosen. The setup needs to emit light in a band with an FWHM of around 10 nm. Therefore filters with high out of band suppression and small transmission band were needed. The out of band parts of the filter should be suppressed in an order of magnitude that the lit instrument cannot detect them. This parameter being individual to each instrument, the EnMAP instrument was used as a reference once again. For it a difference of nine orders of magnitude is considered sufficient. Filters who fulfill these requirements are dichroic bandpass filters, which can be bought from multiple manufacturers such as Newport, Iridian or Thorlabs. From those three companies, Thorlabs provided a wide range of different central wavelengths for the filters as well as the least expensive prices compared to the competitors. For that reason the filters were bought there. The FBH filters of Thorlabs provide an FWHM of 10 nm and an optical density of six. This corresponds to a suppression of the out of band light of six orders of magnitude. In order to achieve nine orders of magnitude a stack of multiple filter of the same type was considered. The filters are available in two

different sizes, namely with a diameter of half an inch or an inch. For this setup only filters with a diameter of an inch were used, since this size offered the biggest variety.

For the filters to be changeable a 3D printed filter wheel with electric motors was constructed. The wheel is depicted in figure 3.3. The wheel allows to install lens tubes with mounted filters into it. Each of the wheels can hold up to 16 lens tubes with a maximum length of one inch. A one inch lens tube can hold up to four filters. The position of the wheel is set via the serial communication port of an Arduino which controls the motors. To distinguish the different positions on a wheel, an optical coupler is used on each one and connected to the Arduino. Every position on the wheel has a small sprocket that shadows the optical coupler, this allows the controlling software to incrementally count while the wheel is rotating. And therefore to control the relative position of the filter wheel.

Figure 3.3: 3D printed filter wheel with Arduino controller.

To be able to adapt to different optical instruments, with according detector sensitivities a second wheel was added. In which neutral density filters can be integrated in order to adapt the optical power output of the source to the corresponding instrument.

As stated above the EQ-99XFC generated light needs to be collimated to be guided through the setup described above. The collimation needs to be wavelength independent in order to align the whole spectrum of the EQ-99XFC. The wavelength independence is provided by the use of metallic mirrors. Manufactures provide different metals. The best suited according to its reflectance was a silver mirror with protected coating, provided by Thorlabs. Its reflectance is depicted in figure 3.4 below. The manufacturer offers a multitude of different parameters for their silver mirrors. The mirrors are classified by their size (in terms of base diameter) and focal length. The different mirrors can be bought in a mounting device with a FC fiber connector, where the fiber core is centrally aligned onto the mirror at a distance of its respective focal length. From this derives the question which of the variety of possible mirrors is best suited for the setup.

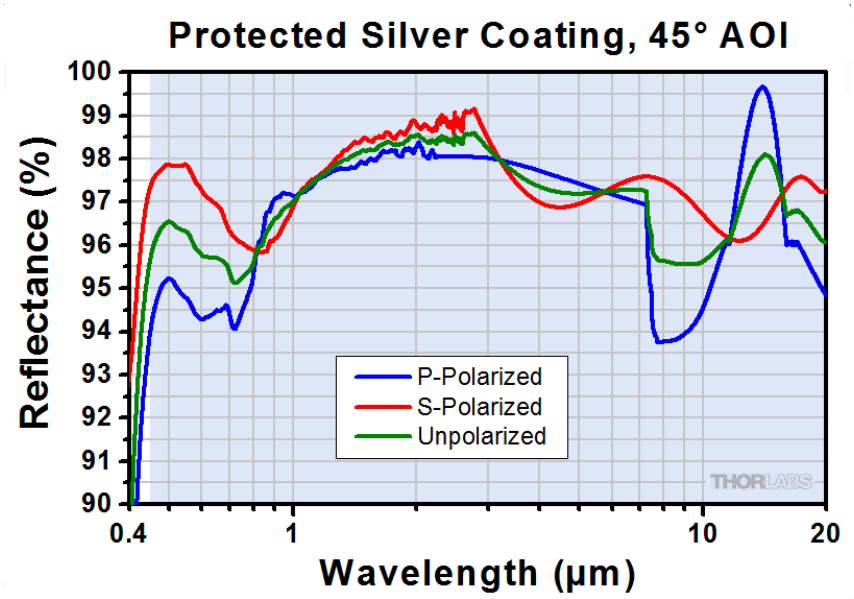

Figure 3.4: Reflectance of protected silver off-axis parabolic mirrors over a spectrum from 0.4 μm to 20 μm taken from the Thorlabs website [17].

The focal length of the mirror influences the diameter of the collimated beam, depending on the numerical aperture of the fiber shining onto it. This relationship can be expressed by the following equation:

$$B_{diameter} = 2 \cdot NA \cdot f_{OAP} \tag{3.1}$$

Where $B_{diameter}$ represents the beam diameter of the collimated beam, NA the Numerical Aperture of the connected optical fiber and f_{OAP} the reflected focal length of the used mirror. The core of an optical fiber cannot be considered as a point light source

therefore in addition the divergence of the beam needs to be considered and calculated. The relation between the core size and the divergence angle is depicted in figure 3.5.

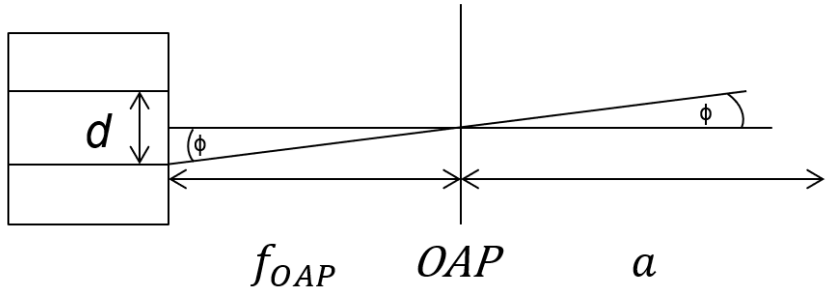

Figure 3.5: Sketch of the beam divergence, where d stands for the fiber core diameter, ϕ for the divergence angle, f_{OAP} for the reflected focal length of the used mirror and a for the optical path length.

The divergence angle ϕ is dependent of the core diameter of the used fiber d and the reflected focal length of the mirror f_{OAP}:

$$\phi = arctan(\frac{d}{2 \cdot f_{OAP}}) \tag{3.2}$$

The divergence angle offers insight on the growth of the diameter of the collimated beam. This influence is shown in equation 3.3 with the addition of the added width of $B_{divergence}$.

$$\begin{aligned} B_{divergence} &= tan(\phi) \cdot a \\ B_{diameter}(a) &= 2 \cdot NA \cdot f_{OAP} + 2 \cdot B_{divergence} \end{aligned} \tag{3.3}$$

As can be seen the beam width increases with the length of the optical pathway. That is the reason why a short optical pathway for the filtering is necessary. Furthermore the reflected focal length has an impact upon the beam diameter as well as the divergence angle. A small focal length mirror produces a smaller beam diameter, which however has a high divergence angle therefore limiting the optical pathway of the setup. The boundary conditions to determine the right mirror was derived from that. Since the beam has to pass filters with a diameter of one inch the beam diameter $B_{diameter}$ can't be greater than 25.4 mm.

A mirror that creates a beam with a diameter below 25.4 mm and allows for an optical path long enough to mount the filter wheels was the half inch off-axis parabolic mirror from Thorlabs. Its reflected focal length of 15 mm creates, in combination with the NA = 0.22 from the light source fiber, a beam diameter of 6.6 mm. After an optical path of 30 cm the beam has a diameter of 10.9 mm according to equation 3.3, which is still below the diameter of the filters. Furthermore the beam diameter needs to be below the diameter of the used mirror which is 12.7 mm. The reason being that in order to conserve

the radiance a fiber with a core diameter of 200 μm was used. In order to get the best coupling efficiency a mirror with the same specs as the one used to collimate the beam is required. This results in the beam being focused on a spot the size of the output fiber.

To be able to adjust the fiber end to the focus plane of the off-axis parabolic mirror the optical fiber was mounted into a translation mount (Thorlabs CXYZ05). The translation mount allows the fiber ends position to be adjusted in X, Y and Z axis. Furthermore to be able to react to slight beam deviations caused small errors in the beam alignment the off-axis parabolic mirror was mounted into a translation stage which permits to adjust the angle at which the beam falls onto the mirror. The translation mounts combined provide five degrees of freedom for the adjustment of the mirrors focal plane.

As connecting fiber between both parts of the setup an optical fiber with FC connector with a 200 μm core diameter and broad transmission spectra was used (Thorlabs FG200LEA).

For the second monitoring part of the setup the beam collimation needs to be reevaluated. Since the output fiber has a rectangular core using a 1:1 image of the round core onto it will lead to losses due to the different geometrics of the cores. Using mirrors with different focal lengths in order produce a smaller image was considered. The smaller image would reduce the losses due to the geometrical mismatch, however the smaller focal length leads to increased angles of incidence of parts of the image. This also causes losses due. Due to the losses of the geometric mismatch being around 15% which was below the losses caused by the angular mismatch the same mirrors as for the filter part of the setup were used.

As stated in section 3.1.2 the beam needs to be split in order to be monitored. To keep losses to a minimum, a splitter with a splitting ratio of 5 to 95 was needed. Furthermore the splitter needed to have a linear transmittance over the spectrum of the light source. These requirements were met by an optical quartz made of Infrasil provided by Thorlabs. Its transmission spectrum is depicted in figure 3.6. The infrasil window reflects 6% over the spectrum from 350 nm to 2500 nm, which meets the necessary requirements. The window was mounted in an angular rotation device in order to guide the reflected part of the beam into the monitoring device.

As a monitoring device the Newport power meter described in section 2.4.4 was used with the 918D-SL-OD3R detector.

To be able to turn the setup output on and off without shutting down the plasma lamp a shutter was needed. The shutter used needed to be controllable via an external trigger signal. This was achieved with the Thorlabs SH1 shutter. The SH1 possesses a one inch aperture and can be controlled via a 5 V TTL signal when connected to the Thorlabs KSC101 solenoid controller.

All components mentioned above were aligned using the Thorlabs 30 mm cage system.

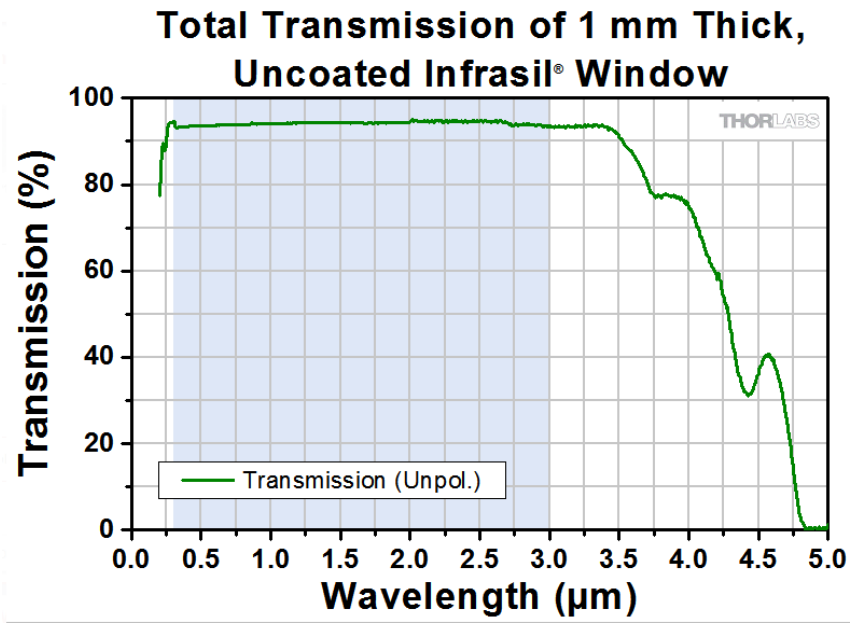

Figure 3.6: Transmission of a 1 mm thick window of Infrasil at normal incidence. Taken from the Thorlabs website.

The light source setup was build using the components selected above. The characterization results for the selected filters and the light source will be discussed individually in section 4. Optical power measurements of the output before the monitoring setup were conducted with the Newport power meter to characterize the coupling efficiencies. The measured setup is depicted in figure 3.7. The resulting power was 30% of the power measured after passing the filters. Therefore the attenuation can be attributed to losses caused by the fiber coupling. Reasons for the losses may be poor imaging of the used off-axis parabolic mirror [11]. Furthermore the degrees of freedom provided by the different mounts may be insufficient to correctly adjust the focal plane to the fiber end.

Due to the poor efficiency the optical power transmitted in the SWIR is insufficient if two fiber couplings attenuations are combined. In order to avoid this the monitoring part of the setup was integrated into the filtering part in order to avoid the attenuation of a second fiber coupling.

3.2 EQ-99XFC characterization

The used light source needed to be characterized power and spectrally wise. This was achieved by the use of two different measurement setups.

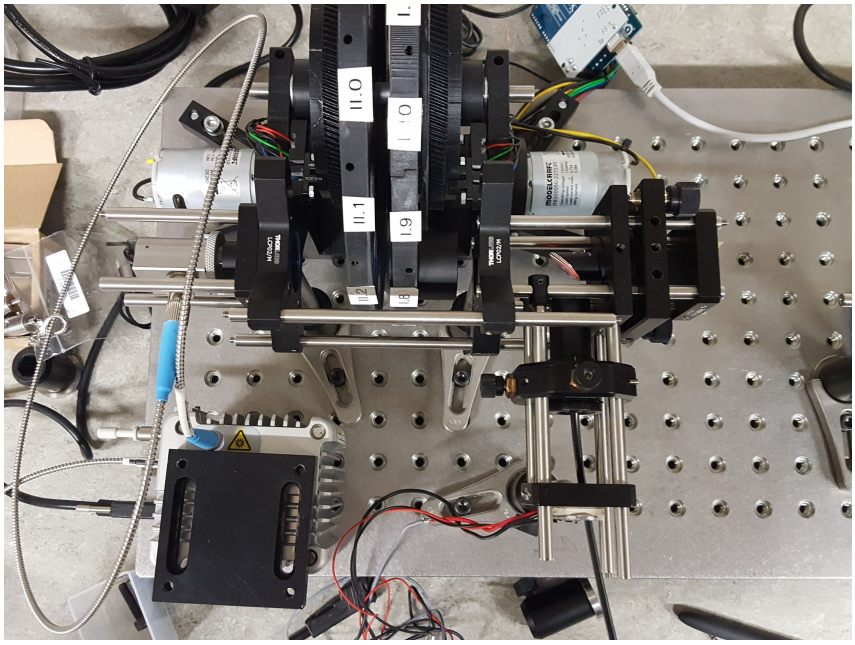

Figure 3.7: Filtering part of the light source setup connected to the Newport power meter.

3.2.1 Measurement of the Spectral power density

To determine its spectral power density the EQ-99XFC's FC fiber output was collimated by an off-axis parabolic mirror with an FC fiber connector (Thorlabs RC04FC-P01). For safety reasons the UV light with wavelengths below 320 nm emitted by the EQ99XFC was filtered with a UV Filter (Newport CGA-320). Afterwards the free ray beam was guided through three dichroic bandpass filters with an FWHM of 40 (Thorlabs FB600-40), to narrow the spectrum. As described in section 3.3 the beam diameter of the free ray increases with distance from the collimator. Due to the limited size of the photo detector, a lens was used to focus the light onto it. The laboratory lights were turned off during measurements. The setup is depicted in figure 3.8.

3.2.2 Spectrum measurement

In order to measure the relative spectrum of the EQ99XFC the HR-1024i Spectrometer, described in section 2.6 was used. As with the spectral power density measurement the light source needed to be collimated. The same setup as described in section 3.2.1 was used for that purpose. The collimator needs to be achromatic for the measured spectra to be accurate. The mirrors reflectance is depicted in figure 3.4 in section 2.3.1. To optimally fill the Field of View of the HR-1024i an optical fiber, provided by the manufacturer, was used.The fiber is depicted in figure 3.9. The collimated beam was targeted at the open fiber end, whereas the other end was connected to the HR-1024i input. To avoid over saturation of the spectrometers detector due to the high radiance of the EQ-99XFC the beam wasn't directly pointed at the fiber end. The laboratory lights were turned off during the measurement.

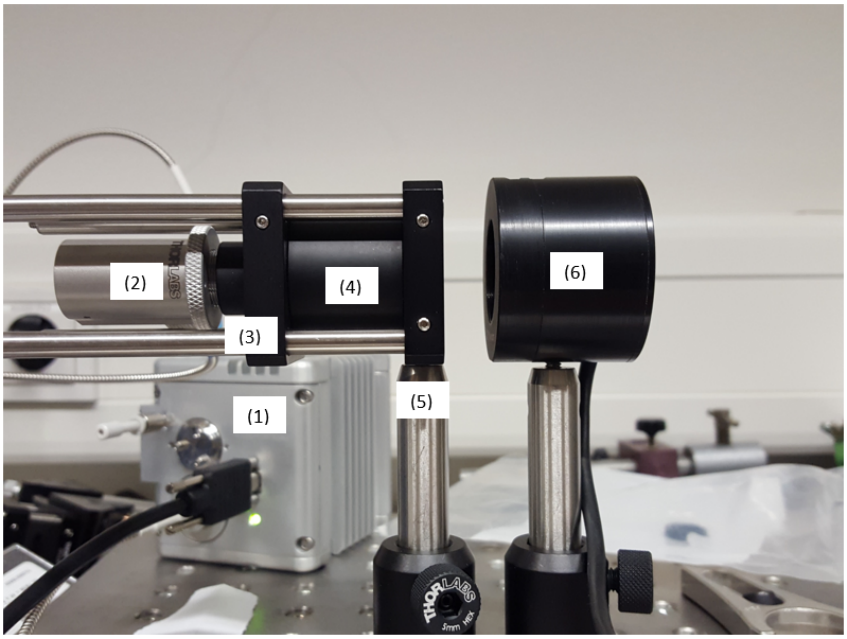

Figure 3.8: Measurement Setup for EQ99XFC power characterization. (1)EQ99XFC light source, (2)RC04FC-P01, (3)CGA-320 UV Filter, (4)FB600-40 Filters, (5)Focusing Lens, (6)Photo detector.

3.3 Filter characterization

Different properties of the dichroic filters needed to be determined. For this purpose, a specific measurement setup was used. This section presents and explains it.

The different filters needed to be tested in regards of the following aspects:

- The conformity with the manufactures data sheets
- The dynamic range between their transmission band and their block band
- The edge steepness of the transmission band

To measure these characteristics the filters were the EQ-99XFC was collimated with the same setup as described in section 3.2.1. The same mirror as used in the collimator was used to couple the light into the fiber connected to the measurement device. The light was guided onto the off-axis parabolic mirror with an dichroic mirror.

A spectrometer with a wide dynamic range and broad wavelength range was needed in order to determine the quality of the out of band suppression of the filters. These conditions were met by an OSA (Yokogawa AQ6374). It provides a dynamic range from +20 dBm to -80 dBm over a wavelength range of 1400 nm from 350 nm to 1750 nm. The whole spectrum of the EQ-99XFC is not covered, however the filters characterized with it are transmissive beyond 1400 nm. Furthermore wavelength resolutions up to 0.5 nm are possible, which is required for the measurement of the filter passband slopes.

Figure 3.9: Optical Fiber provided by Spectra Vision Company.

The AQ6374 has an FC fiber input, therefore the filtered collimated beam needed to be coupled into an optical fiber. Hence the fiber used to couple light into the OSA, needs a broad transmission spectrum. This was achieved by using low OH silica multimode fibers. Due to the OSA resolution depending on the core size of the used input fiber two different fibers were used during the measurements. One with a core diameter of 200 μm and one with 100 μm.

To measure the highest possible dynamic range between the passband and the out of band suppression the power coupling needed to be maximized. This was achieved of the EQ-99XFC output fiber onto the OSA input fiber. Since the EQ-99XFC output fiber has a 200 μm core diameter the fiber with a core diameter of 200 μm was used as input fiber. This allowed to couple in more light into the OSA however limiting its spectral resolution to 1 nm. This is caused by the input optic of the OSA being overfilled according to the manufacturer.

For a detailed measurement of the filters edges a resolution below 1 nm was needed to spectrally resolve the whole edge. This was achieved by using a fiber with 100 μm core diameter, at the cost of absolute power loss compared to the 200 μm core fiber. The smaller fiber allows resolutions up to 0.1 nm.

The measurement setup with the 100 μm core fiber is depicted in figure 3.10.

3.4 Filter angular tuning

To achieve a high optical density the same type of filter was used multiple times in a stack. Due to limitations in the production process the central wavelength of the filters deviates on an order of $+/-2$ nm around the specified wavelength. To optimize the transmission bands of the individual filters relative to each other,

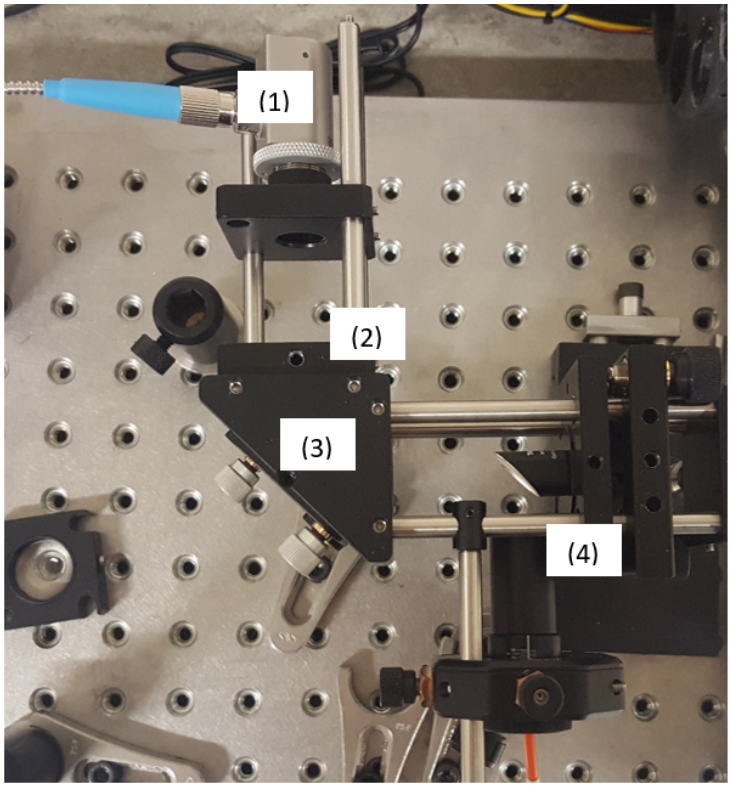

Figure 3.10: Measurement setup of the Filter Characterization: (1)EQ99XFC plugged into collimator, (2)Characterized Filter, (3)Dichroic mirror, (4)Fiber coupling.

their angular dependency was exploited, as described in section 2.3.3. The goal of the measurement was to find an angle for each filter in a manner that their central wavelengths only differ around 0.5 nm from each other in the final stack.

The measurement setup is depicted in figure 3.11. The single filters very mounted onto a precision angular rotation stage which allowed angle changes with 0.1° precision. They were illuminated by the collimated beam of the EQ-99XFC, which was realized with the identical setup as in section 3.2.1. The beam then passed the mounted filter and was attenuated afterwards by a neutral density filter. After which it was coupled into the spectrometer with a wavelength range from 600 nm to 1100 nm (Zeiss MCS 100), via a multi mode fiber with 200 μm core diameter. Measurements were taken in a 1° interval starting at 0° and going up to 10°.

3.5 Optical density characterization

To validate the enhanced optical density of a filter stack the dynamic range provided by the AQ6374 and EQ99XFC was to small with at best six orders of magnitude. With a maximum power ratio measured of -20 dBm for the EQ-99XFC and the noise floor of the AQ6374 being at -80 dBm, which only allows six orders of magnitude. To further investigate it, measurements with two lasers diodes were made to test the optical density at specific wavelengths. Both with comparable power outputs

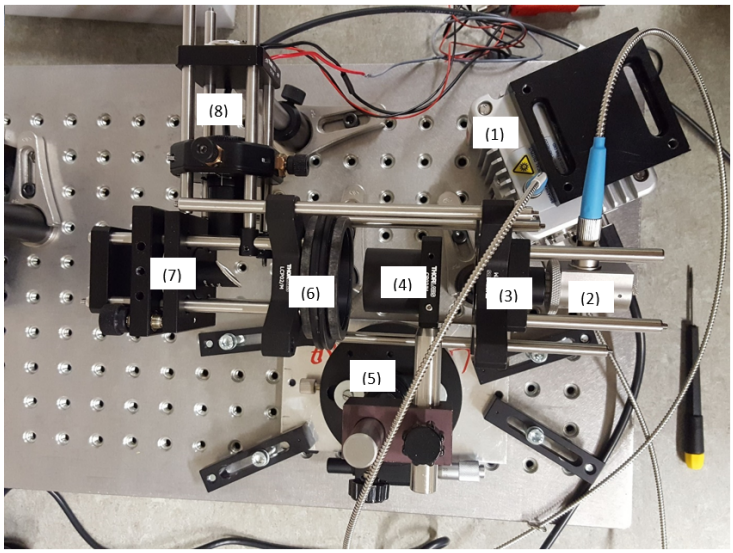

Figure 3.11: Measurement setup of the Angular Filter Tuning: (1)EQ99XFC light source, (2)RC04FC-P01, (3)CGA-320 UV Filter, (4)Filter, (5)Angular Rotation Stage, (6)Neutral Density Filter, (7)THORLABS OAP mirror, (8)Multi mode fiber.

at around 100 mW, with their central wavelengths being at 650 nm and at 950 nm.

The measurement setup for the 660 nm laser is depicted in figure 3.12. This Laser diode was delivered with a focusing optic, which was used to target the laser at the Newport photo detector 2.4.4. In between a lens tube was placed capable of holding up to four filters. The light path was encapsulated to keep the amount of stray light to a minimum. The laboratory lights were also turned off during measurements. The laser diode was powered by a tunable power supply with current control. The operating current was set at a level that the power meter displayed a power of 100 mW when illuminated with the respective laser beams.

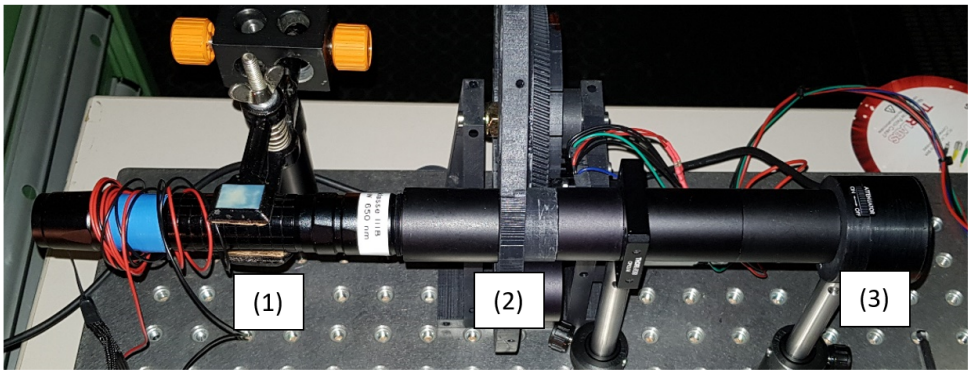

Figure 3.12: Measurement setup for optical density characterization: (1) Laser diode with focusing optic, (2)Mounted filter, (3)Photo detector

4 Results and Discussion

4.1 EQ-99XFC

The Manufacturer of the EQ99XFC provides a data sheet [6] with its spectral power from 180 nm to 900 nm. For the designated purpose of the light source however the spectral power not only in the VNIR but also in the SWIR are needed. In order to characterize the EQ-99XFC, the measurements described in section 3.2 were conducted. Their results will be discussed below.

4.1.1 Spectral power

The spectral power of the EQ-99XFC at 600 nm was measured with the setup described in section 3.2.1.The power meter calibration was set to 600 nm.

The Newport power meter returns an optical power value in Watt. In order to calculate the spectral power from it, the filter attenuation of the measurement setup needs to be taken into consideration. The light coming out of the fiber is attenuated by the UV filter and the interference filters. Since the measured power value is attributed to a specific wavelength the attenuation of the filters can be taken from their respective data sheets.

The UV Filter transmits 98% at 600 nm, the FB600-40 up to 77%. The measured power then needs to be divided by the spectral width of the signal to calculate the spectral power of the EQ-99XFC at 600 nm. The FWHM of three FB600-40 filters is depicted in figure 4.1 and lies at 25 nm. The unattenuated power emitted by the EQ-99XFC at 600 nm can be calculated by the following equation :

$$\begin{aligned} P_{detector} &= P_{EQ-99XFC} \cdot T_{UV} \cdot T_{FB600-40} \\ P_{EQ-99XFC} &= \frac{P_{detector}}{T_{UV} \cdot T_{FB600-40}} \end{aligned} \tag{4.1}$$

$P_{detector}$ represents the power displayed by the Newport power meter, $P_{EQ-99XFC}$ the power emitted by the EQ-99XFC before passing the filters, T_{UV} and $T_{FB600-40}$ the transmission factors of the aforementioned filters at 600 nm.

With $T_{UV} = 0.98$ and $T_{FB6000-40} = 0.77$ and the Newport Power meter displaying $P_{detector} = 1.112\ mW$ this results in the following power at 600 nm of $P_{EQ-99XFC} = 1.47\ mW$. With the FWHM the spectral power can be calculated. $P_{spec} = 58.8\ \mu W/nm$, this corresponds with the value extracted from the manufacturers data sheet [6].

4.1.2 Scaled spectrum

With the measurement setup described in section 3.2.2 the relative spectra of the EQ-99XFC was measured. The spectrum was weighted by the spectral power density at 600 nm calculated above in Eq. 4.1. The resulting spectra is shown in figure 4.2.

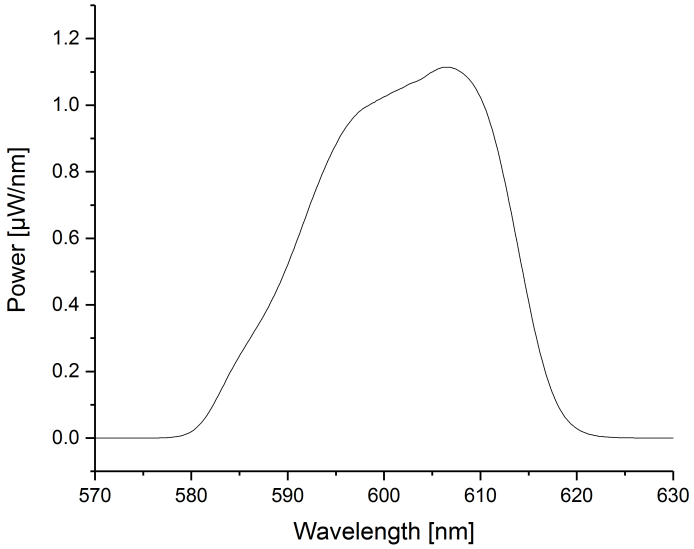

Figure 4.1: Spectrum of the three FB600-40 measured from 570 nm to 630 nm.

The spectrum from 400 nm to 980 nm corresponds to the data sheet given by the manufacturer [6]. The discontinuity at 1900 nm is caused by a switch in detectors in the the SVC. The strengths of the EQ-99XFC in terms of spectral power density lie in the UV region. Which translates to the VNIR, where it exceeds 10 μW/nm. Whereas in the SWIR region it falls from 6 μW/nm at 1400 nm to 2 μW/nm at 2100 nm. The offset due to the detector switch needs to be considered as well, which suggests that the actual power maybe lower in that region.

To provide a better context for the measured spectra, a comparison with a practical example seems appropriate. One application for the final setup will be the stray light calibration of the EnMap Instrument. For this purpose, a certain amount of power for the different detector elements is needed. These are depicted in figure 4.3.

These power levels need to be met by the final setup in order to provide the required calibration. It can be concluded that the EQ-99XFC on its own provides enough power. However, this doesn't account for losses caused by the light source setup which need to be kept at a minimum, especially for the SWIR region where a loss of 10% at 2100 nm is enough that the needed spectral power is not reached.

4.1.3 High frequency modulation

During the power measurement with the Newport power meter a sinusoidal modulation was found with a frequency of 44 kHz, this is depicted in figure 4.4. This is caused by the electronic drivers of the pumping laser of the EQ-99XFC. For the purpose of this setup the modulation influence is limited. Since the estimated in-

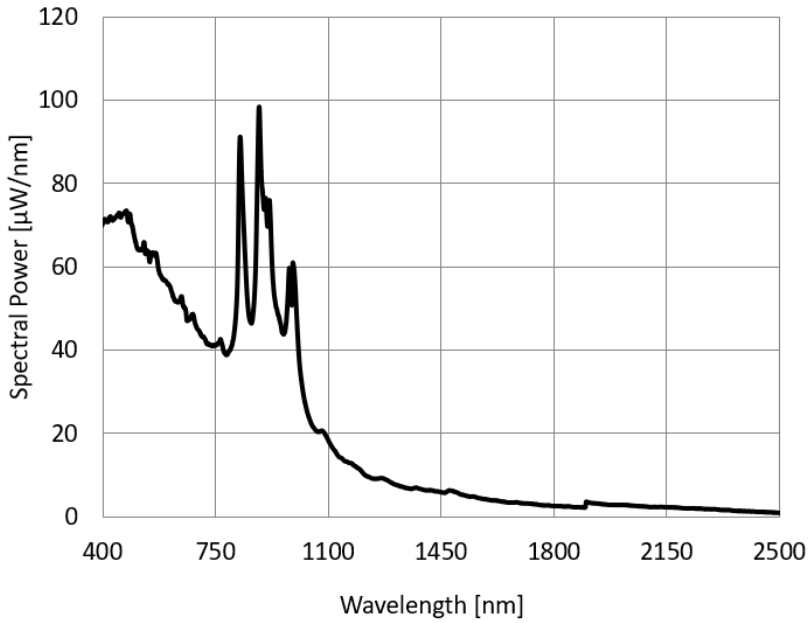

Figure 4.2: Spectrum of the EQ-99XFC measured by the SVC 1024i and weighted by the Newport power meter measurement.

tegration time of the measurements taken with this device will be in time scales of multiple milliseconds and therefore the modulation influence will be averaged out.

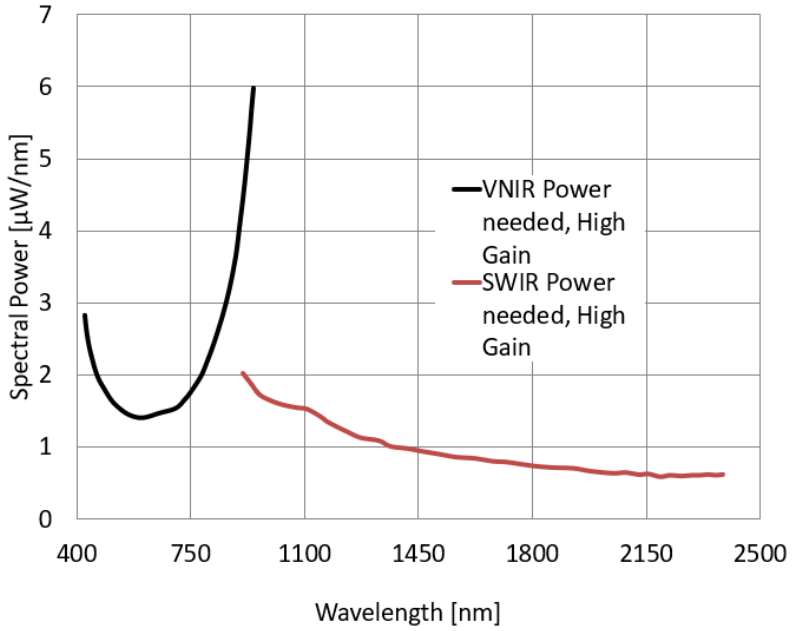

Figure 4.3: Estimated spectral Power needed for the Stray light calibration of the EnMAP VNIR and SWIR detectors set to high gain.

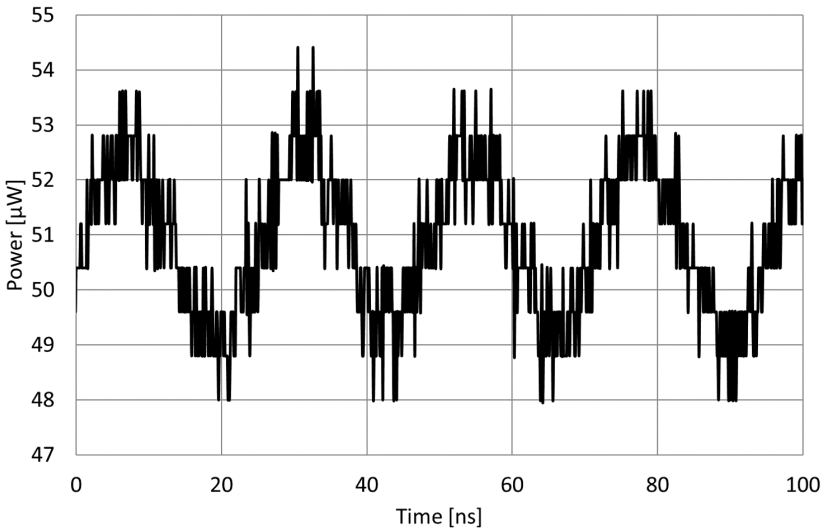

Figure 4.4: Power of the EQ-99XFC measured with the Newport Power meter, over the course of 100 ns.

4.2 Filters

To obtain a spectrally narrow output light, the EQ-99XFC needs to be filtered. In order to do so interference filters as described in section 2.3.3 were purchased. The individual filters were selected from the same batch by the manufacturer in order to ensure identical coating structures and overlapping central wavelengths of their respective transmission band.

To be used in the light source setup the filters were characterized using the measurement setup described in section 3.3. The focus layed on out of band suppression, transmission band overlap and their edge steepness. In the curse of this thesis 9 different filters were measured. Six with transmission bands in the VNIR. These were the following sorted by their central wavelength and their FWHM:

- 450 nm, 10 nm FWHM (FBH450-10)
- 532 nm, 10 nm FWHM (FLH532-10)
- 660 nm, 10 nm FWHM (FBH660-10)
- 780 nm, 10 nm FWHM (FBH780-10)
- 850 nm, 10 nm FWHM (FBH850-10)
- 950 nm, 10 nm FWHM (FB950-10)

To maintain oversight the results won't be discussed for each filter individually. A summary will be provided and all plots for the different filters can be found in the appendix, including the measurements of the individual filters of the different types and the results of the stacking.

In the first part the transmission band and its overlap of the different filters will be discussed. Then in the second part the edge steepness measurements will be discussed. And in the final third part the effects of filter stacking on the optical density shall be discussed.

4.2.1 Transmission band and central wavelength

According to their respective data sheets all filters purchased are expected to block the VNIR to at least three orders of magnitude, depending on filter quality. As an example, the transmission band of the FBH450-10 depicted in figure 6.1 shall be discussed.

To characterize the magnitude of the out of band suppression a measurement of the unfiltered signal of the EQ-99XFC was done. The relative spectra of the EQ-99XFC in the region from 400 nm to 750 nm is in agreement with the spectra measured in section 4.1.2. The power of the unfiltered EQ-99XFC at 600 nm lies at -20 dBm which corresponds to 10 μW. The difference in power has multiple reasons. For one the power measured in the OSA is resolution dependent. In order to obtain a higher resolution, the entrance slit is narrowed which leads to less

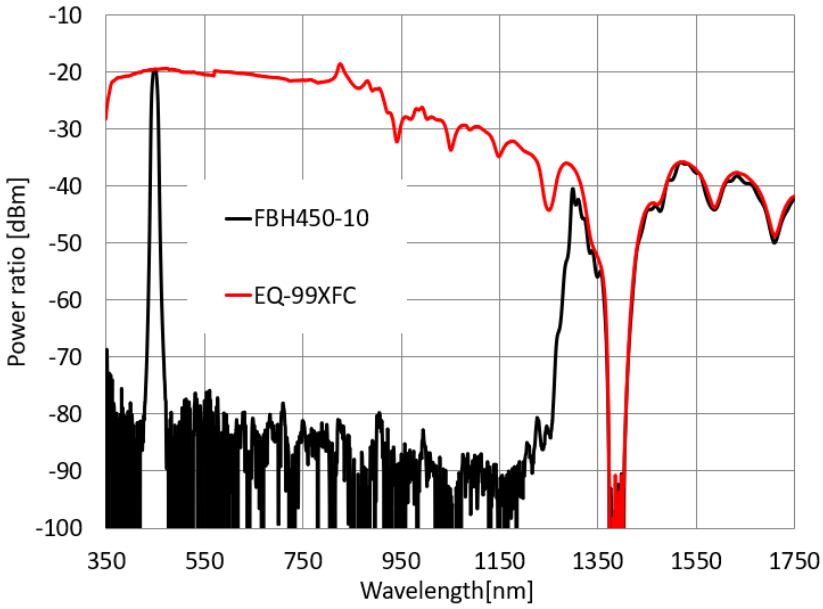

Figure 4.5: Spectrum of the FBH450-10 filter and the EQ-99XFC over the full range of the AQ6374 OSA.

light reaching the detector. Furthermore, the fiber used to couple the light into the OSA has a numerical aperture of 0.22. The input optic in the OSA, has according to the manufacturer, a smaller aperture. This mismatch also causes power losses.

The differences of the relative spectra in the region from 750 nm to 1750 nm compared to section 4.1.2,can be attributed to the dielectric mirror used during the measurement. This mirrors reflectance in this wavelength region matches the differences compared to the measured spectra with the SVC 1024i. However the drop at 1400 nm cannot be attributed to known characteristics of the EQ-99XFC, the mirror or the documented behavior of the AQ6374. The dip was present in all measurements conducted for the VNIR filters. A possible reason is an undocumented measurement artifact of the AQ6374.

A single FBH450-10 filter performs accordingly to its data sheet. The filter transmission band has a width of 10 nm at its FWHM. At -80 dBm its width is 40 nm broad. The light of the EQ-99XFC is suppressed to the AQ6374 noise level until 1200 nm, were the filters start to be fully transparent for the incoming light. The stop in light suppression around 1200 nm is observed for each of the VNIR filters. The high transmission in this region needs to kept in mind. The EnMAP instrument at which the light source will be pointed isn't sensible in that spectral area according to figure 4.3. Another possibility may be adding a cut-off filter for wavelengths over 1000 nm, such as the FES1000 provided by Thorlabs.

From 350 nm to around 1100nm nm an out of band suppression of at least six orders of magnitude is observed for the FBH450-10. The goal for the out of band suppression was set at nine orders of magnitude. From this measurement this cannot be verified. The setup is limited by the noise floor of the AQ6374 at -80 dBm

and the maximum power of the EQ-99XFC coupled into it, at around -20 dBm. Therefore the dynamic between signal and noise is limited to six orders of magnitude.

Analog to the FBH450-10 the other VNIR filter plots were analyzed. The individual orders of magnitude for the out-of band suppression given for the different filters refers to the interval from 350 nm to 1100 nm. The only other filter to achieve an out of band suppression of at least six orders of magnitude is the FBH660-10. The FLH532-10, FBH780-10 and FBH850-10 block five orders of magnitude. The FB950 however only suppresses three orders of magnitude. The results are summarized in table 1 below.

Filter	Out of Band suppression
FBH450-10	6
FLH532-10	5
FBH660-10	6
FBH780-10	5
FBH850-10	5
FB950-10	3

Table 1: VNIR Filters and their respective out of band suppression in orders of magnitude. in the interval from 350 nm to 1100 nm

SWIR filters For the SWIR Filters only samples were ordered. Two samples were characterized, both with similar central wavelengths of their transmission band at 2100 nm. However, their transmission band width were different. The AQ6374 spectral range only goes to 1700 nm, therefore another OSA with detectors in SWIR region was needed. The AQ6374 in the measurement setup in section 3.3 was replaced with the Yokogawa AQ6376. The AQ6376 has detectors sensible for wavelengths from 1500 nm to 3400 nm. The spectra of the two filters are depicted in figure 4.6. The filters suppress the out of band signal over 4 orders of magnitude in the measured spectrum from 1500 nm to 2500 nm compared to the EQ-99XFC signal.

Transmission band overlap The difference between the individual filters of the same type lies in the central wavelength of their transmission bands. By the manufacturer the standard deviation is given by $+/-$ 2 nm. Even though the filters were taken from the same batch their central wavelengths differ in the interval cited before.

In case of the FBH450-10 the individual central wavelengths only differ by a maximum of 0.5 nm. This is depicted in figure 6.2.

However, the other filters differ much more in this regard. The largest deviation is observed for the FBH850-10 were the difference reaches 4 nm between single filters. This is depicted in figure 4.8. The other filters range somewhere in between those two cases. The deviation of the other filters is documented in table 2. The missing overlap of the

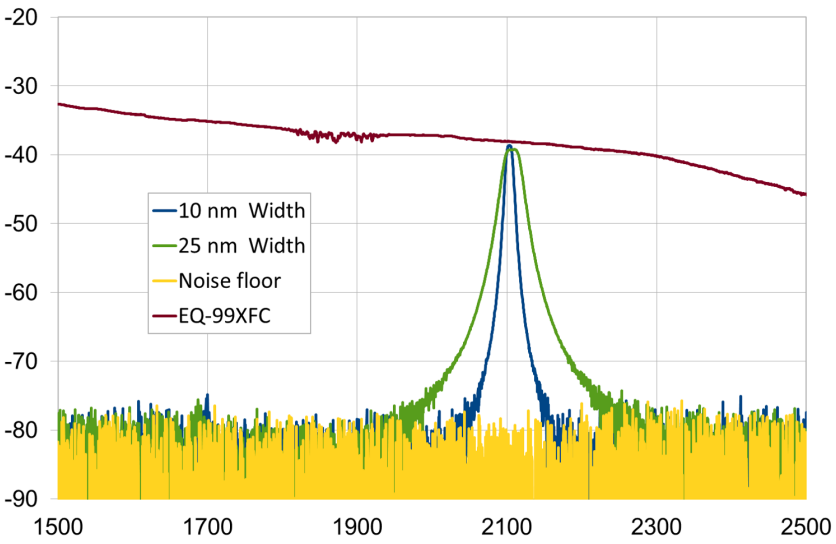

Figure 4.6: Spectrum of the SWIR filters and the EQ-99XFC from 1500 nm to 2500 nm.

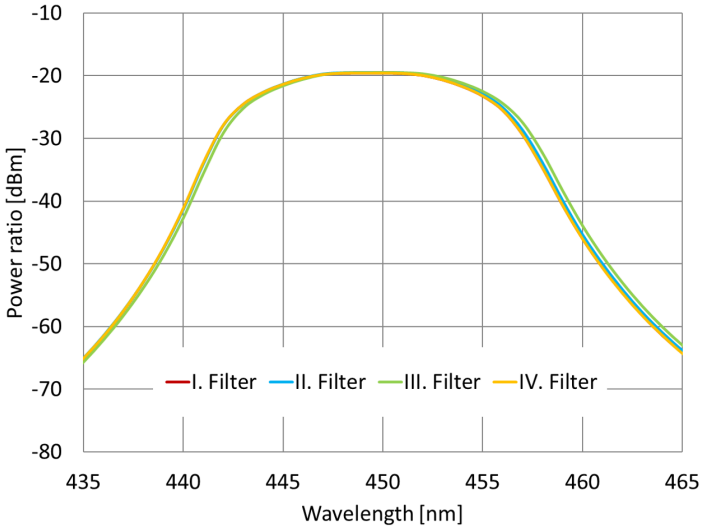

Figure 4.7: Passbands of the four FBH450-10 filters from 435 nm to 465 nm.

individual transmission bands affects the transmission band of the filters in a stack. This leads to the next section, the discussion of the edge steepness of the stacked filters.

4.2.2 Edge steepness of the transmission band

As discussed in section 4.2.1, the transmission band width of the filters broadens beyond 10 nm for lower energies. To reduce this and improve their out of band suppression the same filter is stacked four times. This influence was measured; the setup was described in section 3.3. The results will now be presented and discussed.

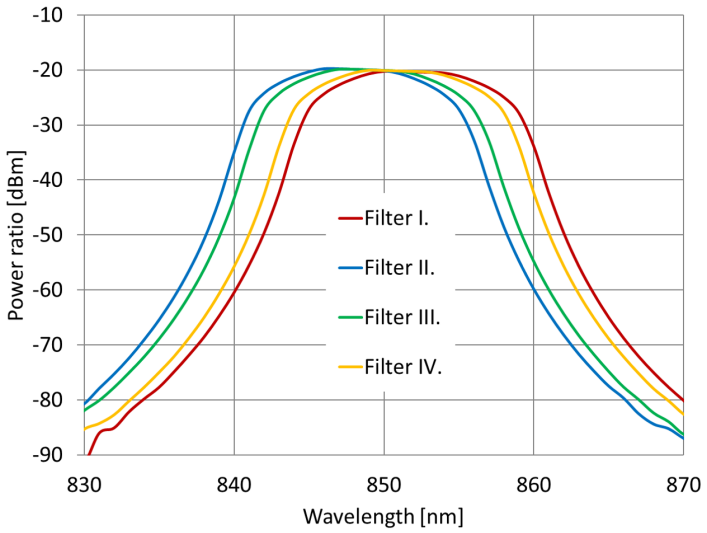

Figure 4.8: Passbands of the four FBH850-10 filters from 830 nm to 880 nm.

Filter	Max central wavelength deviation [nm]
FBH450-10	0.5
FLH532-10	2
FBH660-10	1
FBH780-10	3
FBH850-10	4
FB950-10	1

Table 2: Central wavelengths deviation between the individual VNIR Filters.

In order to correctly determine the effects of the stacking, the slopes of the transmission band were measured. To characterize them appropriately the measurement resolution was set to 0.5 nm. This was achieved by using an optical Fiber with a core diameter of 100 μm instead of 200 μm. The smaller fiber core as well as the higher resolution reduces affect the power measured by the OSA. The missing power reduces the achievable dynamic between the transmission band and the noise floor. Therefore, an direct improvement of the out of band suppression cannot be determined by this measurement.

As in the previous section, distinct filters will be discussed to maintain an oversight. Since the FBH450-10 filters provided the best CWL overlap of the measured group, with only a deviation of 0.5 nm, they provide the best analytical ground for the effects of filter stacking.

The figure 6.3 depicts the results of multiple filter stacking. Figure 6.3 is logarithmic. As stated above the maximum measured power declined from -20 dBm to -37 dBm.

The width of the respective transmission bands for one, two and three FBH450-10 filters increases with the number of filters used. However,

adding a fourth doesn't improve the edge steepness of the slopes any further.

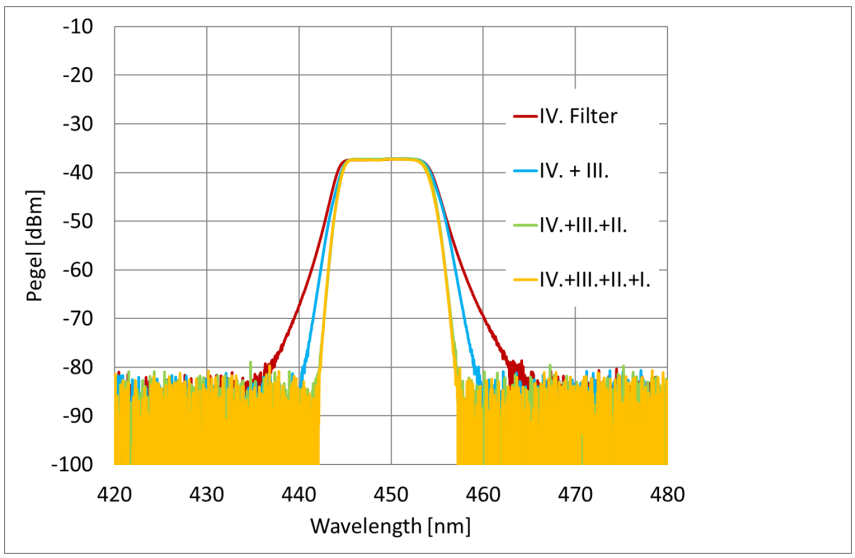

Figure 4.9: Edge Steepness of FBH450-10 filters measured from 420 nm to 480 nm, compared between one and a stack of two, three and four filters on a logarithmic scale.

The biggest impact can be observed from joining two filters. The width of the transmission band decreases from 30 nm at -80 dBm to 18 nm. Adding a third filter the width is reduced to 15 nm. Adding a fourth filter has no measurable impact on the transmission band width.

From the measurements in section 4.2.1 a theoretical curve was calculated in order to estimate the effect of multiple filters in stack. From the measurements of the individual FBH450-10 filters a transfer function could be calculated for each filter. From those transfer functions the curve depicted in figure 2.3.3 was generated. Since the measurements in section 4.2.1 were conducted with a resolution of 1 nm, the maximum power is higher and therefore the spectral width of the filter stacks are different from those in figure 6.3. The calculated curve is compared to the measured behavior of two filters. As can be seen the curves differ greatly in terms of transmission band width at lower power levels. The ideal filter stack has a width of 20 nm compared to 30 nm of the measured one at -80 dBm.

The difference between theoretical and measured curve can be traced to reflections between the filters. Since both sides of the filter reflect light. The reflected light by the second filter is reflected back onto it by the first filter, which leads to more light being transmitted.To reach the same out of band suppression as the theoretical combination of two filters, four filters need to be stacked.

The influence of stacking multiple filters on the FWHM of the transmission spectrum is much smaller, the transmission band narrows around 0.5 nm from one filter compared to four, this is depicted in figure 4.1. This narrowing can also be attributed

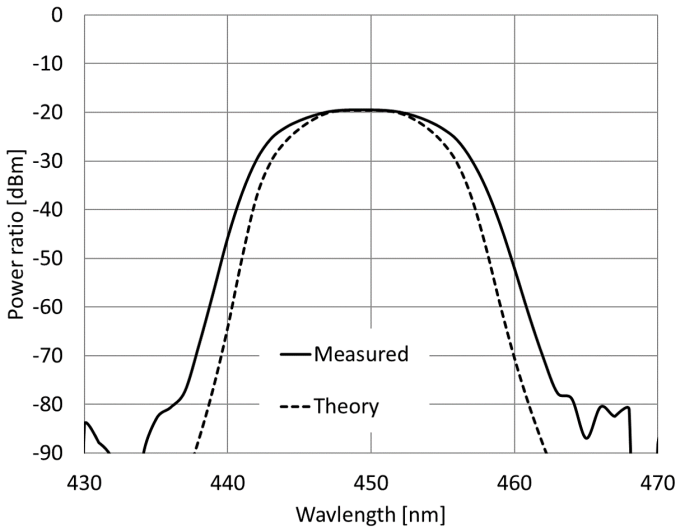

Figure 4.10: Comparison between calculated edge steepness of two FBH450-10 filters and the measured curve.

to the 0.5 nm mismatch between the filter central wavelengths, described in 4.2.1.

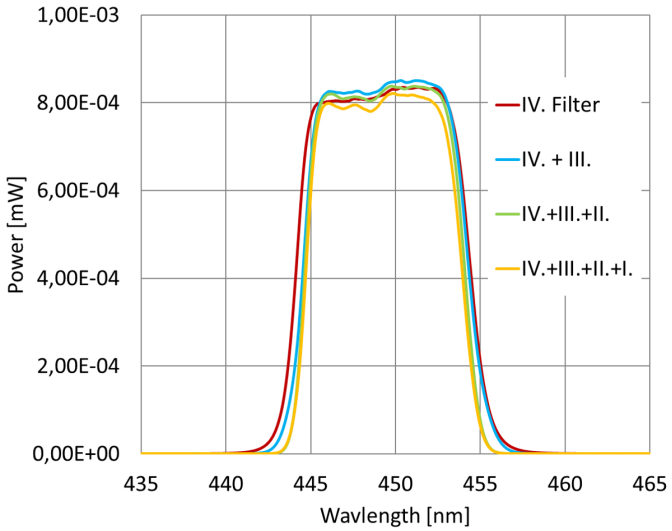

Figure 4.11: Edge Steepness of FBH450-10 filters measured from 435 nm to 465 nm, compared between one and a stack of two, three and four filters on a linear scale.

The missing overlap between the central wavelengths is affecting the edges of the transmission band. The individual FBH850-10 filters showed the highest deviance between their central wavelengths, and the results of their stack will be discussed. The measurement results are depicted in figure 4.12.

As depicted in figure 4.12 the edge steepness isn't symmetrical. The left and right edges slopes differ depending on the number of filters stacked. The symmetry is

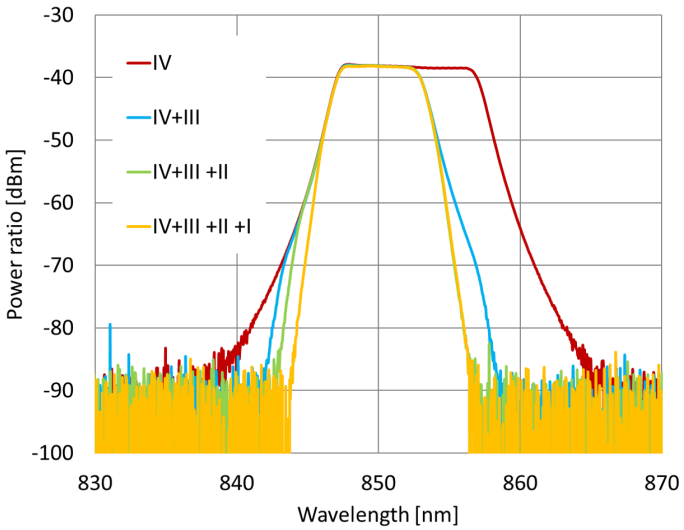

Figure 4.12: Edge Steepness of FBH850-10 filters measured from 830 nm to 870 nm, compared between one and a stack of two, three and four filters on a logarithmic scale.

intact if only one filter is used. Adding a second however cuts the spectral width by 4 nm due to the missing overlap of their transmission bands. The left edge slope is similar to the slope of a single filter until 843 nm where it increases compared to one filter.

The addition of a third filter improves the slope of both edges. The slopes are still non linear. The addition of a forth filter doesn't affect both edges in a symmetrical matter. The right edge is identical to the edge measured with three filters. The left slope is slightly improved compared to three filters.

In order to get symmetrical slopes for the filter transmission band edges the central wavelengths of the filters used in the stack need to be aligned. This will be the topic of the next section.

4.2.3 Filter tuning

As described in section 4.2.1 the central wavelengths of the individual filters of the same type differ up to 4 nm from each other. The effects of this deviation were discussed in section 4.2.2. To reduce this difference, the angular dependency of the filters, described in section 2.3.3, was exploited.

The filters chosen to be analyzed were the FBH850-10 filters since they showed the highest deviation between them, with a difference of up to 4 nm. Since the interference filters shift to lower wavelengths with a changing angle of incidence and therefore to lower wavelengths the filter with the highest wavelength was chosen to be analyzed. The filter in question was filter I with a central wavelength of 852 nm.

Goal of the measurements was to find an angle at which the central wavelength of filter I only differs by 0.5 nm with the filter with the smallest measured central wavelength. In this interval the effect of stacking multiple filters is linearly enough, as discussed in section 6.3 . This was filter II. where it was determined to be at 848 nm. In order to achieve this the incident angle of the collimated beam was changed to the optical axis in steps of 0.5° . The measured transmission bands are depicted in figure 4.13.

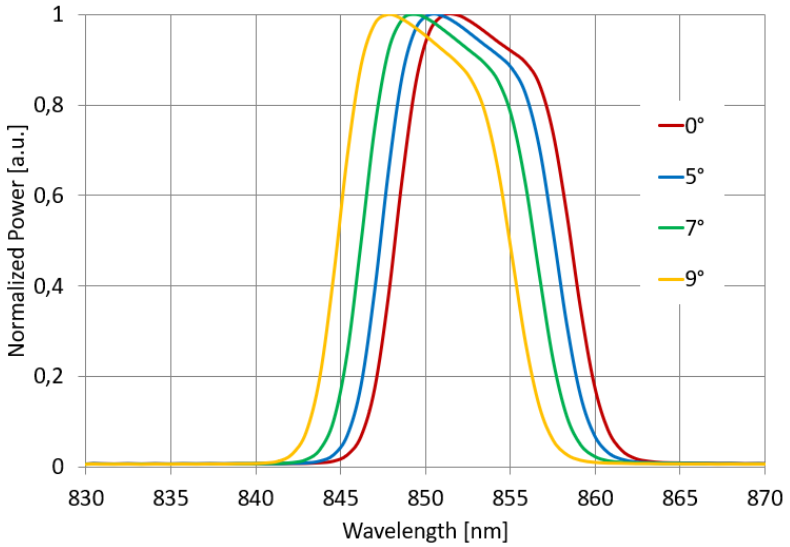

Figure 4.13: FBH850-10 filter number I. under different angles of incidence. From 830 nm to 880 nm. Power normalized without units.

The figure depicts the normalized spectrums measured by the Zeiss spectrometer 2.4.2 for the FBH850-10 filter at different angles of incidence. The spectrum was recorded from 830 nm to 880 nm. As predicted the central wavelength of the FBH850-10 shifts with increasing angles. The effect is minimal below 5° . From 0° to 5° the central wavelength only differs about 1 nm from 852 nm to 851 nm. However starting from 5° the angular dependency becomes stronger. From 5° to 9° the central wavelength changes from 851 nm to 848 nm.

The central wavelength of filter I. reaches 848 nm at 9° . Therefore the set goal of optimizing filter I. towards filter II. was reached in the set interval of 0.5 nm. From this can be concluded that the transmission band of filter I. and II. overlap with a deviation of their centers with less than 0.5 nm if the collimated beam hits filter II. at an angle of incidence of 0° and filter I. at an angle of 9° . The relation between wavelength and angle of incidence can be described by the following equation [1]:

$$\lambda = \lambda_{max}\sqrt{1 - \frac{sin^2\theta}{n_{eff}^2}} \tag{4.2}$$

Where λ describes the wavelength of the filter depending on the angle of incidence θ, the wavelength λ_{max} at $\theta = 0°$ and its index of refrac-

tion n_{eff}. According to [1] n_{eff} can be approximated with $n_{eff} = 2$.

With equation 4.2 and the data obtained by the measurement the remaining filters can be adapted to each other in an analogous manner. As with filter I. the difference between their central wavelengths and that of filter II. needs to be corrected. Filter IV. deviates by 3 nm with a central wavelength of 851 nm and filter III. deviates by 1 nm at 849 nm.

From the data gained, filter III. needs to be tilted by 5° and filter IV. by 7° . With this a custom lens tube was produced using a 3D printer. In it, each filter has its individual position with the needed angle of incidence towards the collimated beam. With this the transmission bands of the different filters align and meet the condition, formulated above, of a deviation below 0.5 nm from the central wavelength for the FBH850-10.

In order to replicate the results for the other filters the same measurements were made with the four FBH780-10 filters. As with the FBH850-10, the filter with the highest wavelength was chosen and tilted until the shortest central wavelength measured in section 4.2.1 was achieved. The filter used was filter IV. with a central wavelength of 780 nm. The wavelength to be achieved was 778 nm, taken from filter I. The results are depicted in figure 4.14.

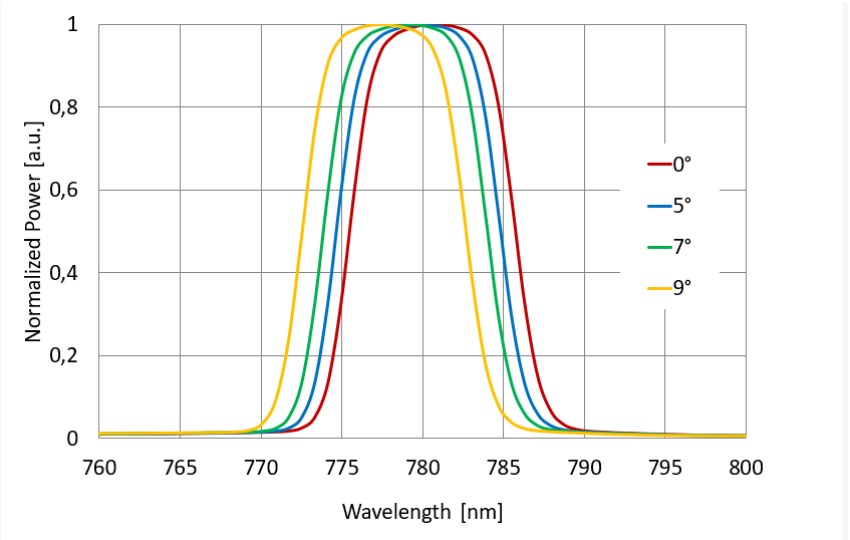

Figure 4.14: FBH780-10 filter number IV. under different angles of incidence. From 760 nm to 800 nm. Power normalized without units.

As with the FBH850-10 filters between an angle of incidence between 0° and 5° the change in the central wavelength is small, it lies around 1 nm. For angles above 5° , same as for the FBH850-10, the center wavelength shifts become bigger. From 1 nm at 5° to 3 nm at 9° . From equation 4.2 an angle of 8° is needed to shift the filter by 2 nm which is confirmed by the measurements.

Remark Refraction of the collimated beam passing through the filters caused by the tilting needs to be considered. The wavelength independancy of this setup cannot be maintained if each filter stack requires a dratic optimization of the fiber coupling.

To examine this an image of the fiber core output of the measurement setup was created. This was achieved by using a lens to create an enlarged image of the core. This image was projected onto the Newport optical power meter. The resulting power was measured with the equivalent wavelength setting and an average was calculated. The results are presented in table 3. A decrease in a size of 1 μW can be observed from 0° to 10° , however a significant drop cannot be observed.

Angle of incidence [°]	0	5	10
Average Power [μW]	50.9	50.4	50

Table 3: Average power of the fiber core at different angles of incidence.

The decrease in optical power indicates that the trajectory of the beam is altered. However the effect of this altering can be neglected for the final setup.

From the measurements discussed above, it can be concluded that it is possible to align filters with missing transmission band overlap. However even though the relation proposed by [1] offers a good approximation the filters still need to be measured to offer certainty in order to reach the goal of a center wavelength deviance below 0.5 nm. In the perspective of new filters being added to the light source setup a guideline on the filter tuning is proposed. After the central wavelength of the filters is determined an approximation of the tilting angle can be done with equation 4.2. Measurements starting from the calculated angle can be done in order to determine the correct angle.

4.2.4 Optical density

As described in section 4.2 the filters need to suppress up to nine orders of magnitude outside their transmission band. To characterize the filter behavior in that regard the measurements conducted prior proved that most filters were capable of at least suppressing six orders of magnitude. The measurements however were limited by the power of the EQ-99XFC. In order to further investigate the out of band suppression of the filters, they were illuminated with the laser diodes with powers over 100 mW. The measurement setup used is explained in section 3.5. The results of the measurements shall be discussed below.

First the different filters were illuminated with the 660 nm laser diode. The noise level was recorded before each measurements to be able to subtract it. With the 660 nm laser all VNIR filters except the FBH660-10 were measured. Since the FBH660-10 transmission lies at 660 nm the out of band suppression cannot be measured with this laser diode. The noise floor of the Newport power meter was determined at 100 pW. With the power of the laser being at 100 mW

this gives a difference of 10 orders of magnitude between signal and noise floor.

From each VNIR filter type first one filter and afterwards four stacked filters were illuminated at an angle of incidence of 0° by the laser diode. The results from section 4.2.1 were confirmed that a single filter can block up to six orders of magnitude. The results of the stack of four filters of the same type was different depending on the filters.

If four filters of the type FBH450-10 and FLH532-10 are stacked and illuminated the power meter doesn't show any signal. Therefore these filters block at least 10 orders of magnitude which meets the set goal of 9 orders of magnitude for these two filter types at 660 nm. After four of the FBH780-10, FBH850-10 and FB950-10 were illuminated the power meter measured power values around 5 nW. From this can be concluded that those three filters block up to 9 orders of magnitude at 660 nm.

From these measurements can be concluded that each of the VNIR filters, except the FBH660-10, meets the goal of an out of band suppression of 9 orders of magnitude at a wavelength of 660 nm. To further investigate the measurement was conducted with an LED laser with a wavelength of 960 nm. This allows the measure the FBH660-10 filters.

As with the 660 nm laser the filter stack of FBH450-10 and FLH532-10 didn't show any signal on the power meter and neither did the filter stack made of four FBH660-10. For the four FBH780-10 filters a power around 5 nW was measured again. The FBH850-10 however transmitted up to 100 nW and didn't show any difference between a single filter and a stack of four. The reason for this can be seen in figure 4.15. The spectrum of the LED laser was measured using a similar OSA as the one used in section 3.3. The emission spectrum of the laser broadens heavenly below a certain level of power. The spectrum becomes so broad that it still emits at 850 nm were the filter transmission band lies, which explains the high transmission of the four stacked filters.

The FB950-10 filters weren't measured due to their transmission spectrum lying in the emission spectra of the laser.
In conclusion to this measurement the improved optical density of a stack of VNIR filters was verified for specific wavelengths. The goal of blocking up to 9 orders of magnitude which each filter was met for the two separate wavelengths. However a conclusion for their whole spectra cannot be conclusively drawn. As depicted in figure 6.1 from section 4.2.1 the out of band suppression of the filters isn't linear. In order to characterize the out of band suppression of a filter stack for the whole VNIR spectrum more measurements may be necessary.

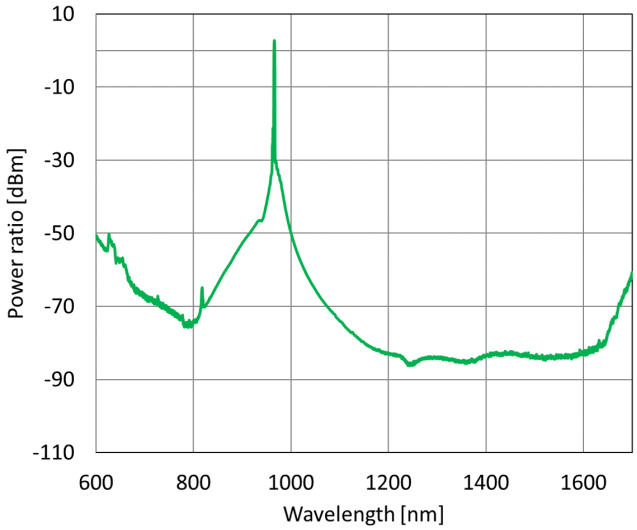

Figure 4.15: Spectrum of the 960 nm LED laser measured from 600 nm to 1700 nm.

5 Conclusion and Outlook

The goal of this thesis was to build a light source setup capable of performing the necessary measurements to support the stray light calibration of array spectrometers. To do so, the necessary requirements for such a light source were formulated. From thereon, different possible light sources were considered. For the most fitting, the EQ-99XFC, a specific setup was designed to meet the formulated requirements.

In order to confirm the assumptions of the theorized setup the setup was built and its crucial parts were characterized. First the EQ-99XFC was characterized in terms of power and emission spectra. These measurements confirmed its adequacy for the setup. For the setup to emit spectrally small near monochromatic light, nine different interference filters types were characterized in terms of their transmission band and out of band suppression. The filters were measured individually as well as in a stack of multiple filters. The measurement results for the individual filters were according to their theoretical specifications. However, a mismatch between the central wavelength of the different filters of a certain type was found. This lowered the out of band suppression of multiple filters in stack; this was addressed and a method to correct it was presented. The improved out of band suppression of multiple filters was investigated at specific wavelengths using laser diodes.

In conclusion an auto automatable light source was built which emits six different characterized spectras. The spectras have an FWHM of 10 nm and are centered around the respective wavelengths of the used VNIR filters: 450 nm, 532 nm, 660nm, 780nm, 850nm, 950nm. They provide an out of band suppression of at least six orders of magnitude for the spectrum from 350 nm to 1100 nm and are estimated to be over nine at wavelengths of 660 nm and 960 nm.

In order to further improve the setup, different points can be addressed. For one the fiber coupling efficiency of the off-axis parabolic mirrors in the setup needs to evaluated and characterized. At the current state, the low efficiency limits the use of the light source in the SWIR region of the spectrum. Further on more filters can be implemented into the setup, using the methods described in this thesis, in order to allow more output options, notably in the SWIR region of the spectrum were only samples were tested. To confirm the out of band suppression of the filters for more wavelengths, measurements with a tunable laser source may provide the required validation.

6 Appendix

6.1 FBH450-10

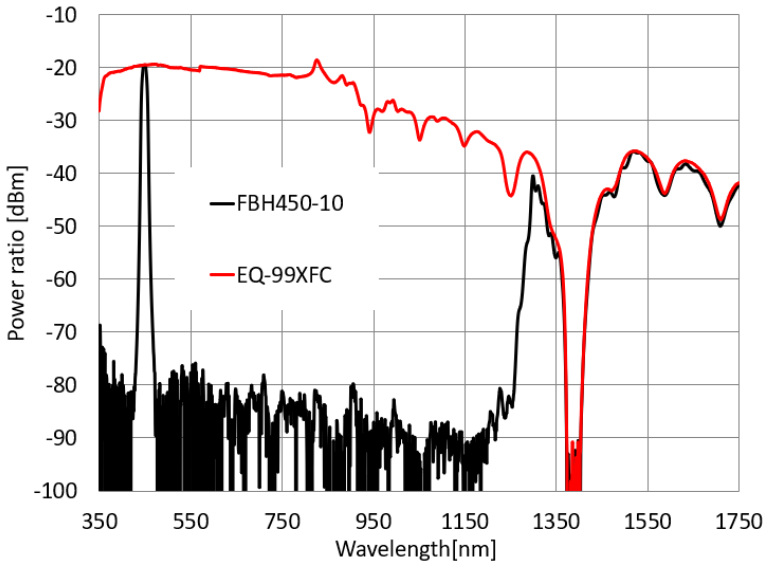

Figure 6.1: Spectrum of the FBH450-10 filter and the EQ-99XFC from 350 nm to 1750 nm.

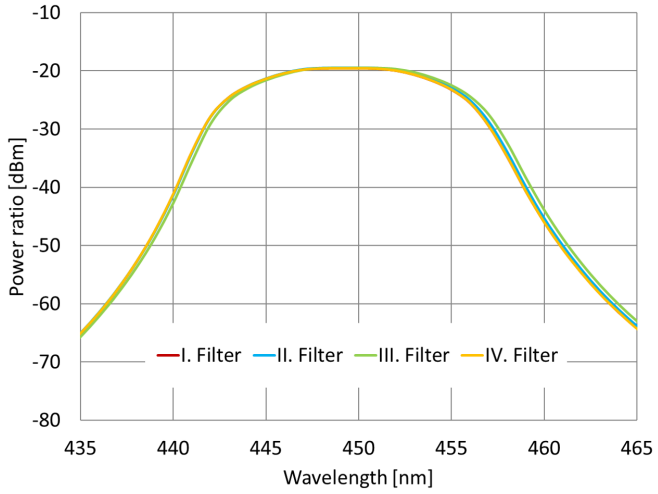

Figure 6.2: Passbands of the four FBH450-10 filters from 435 nm to 465 nm.

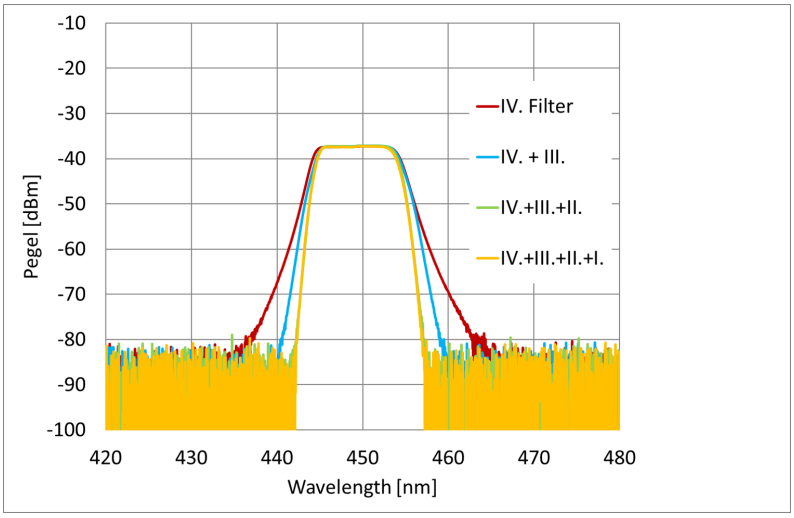

Figure 6.3: Edge Steepness of FBH450-10 filters measured from 420 nm to 480 nm, compared between one and a stack of two, three and four filters on a logarithmic scale.

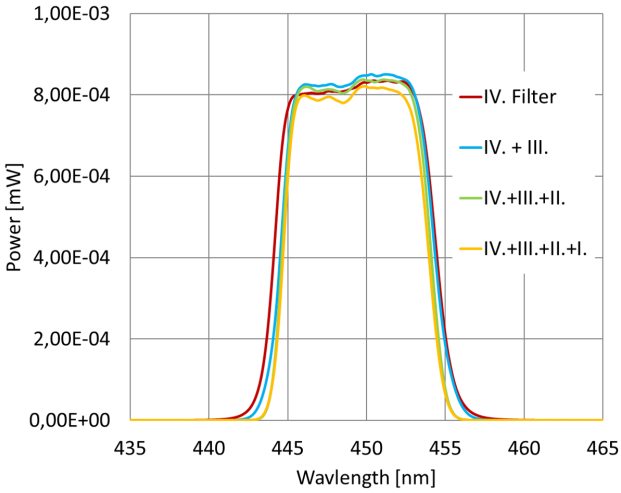

Figure 6.4: Edge Steepness of FBH450-10 filters measured from 435 nm to 465 nm, compared between one and a stack of two, three and four filters on a linear scale.

6.2 FLH532-10

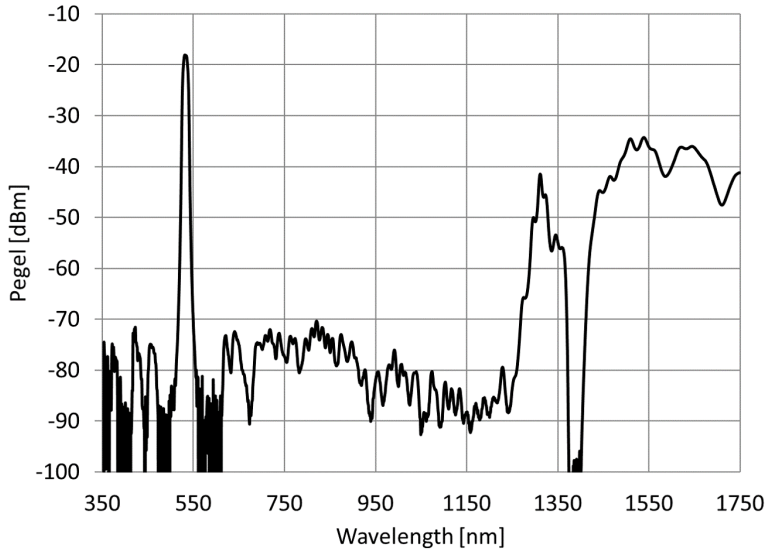

Figure 6.5: Spectrum of the FLH532-10 filter from 350 nm to 1750 nm.

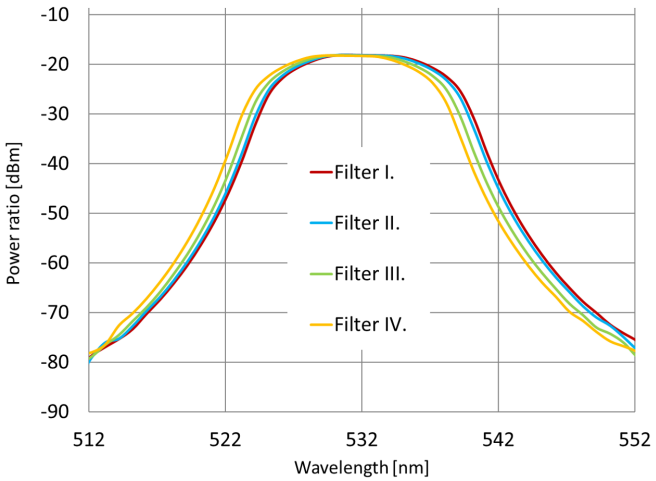

Figure 6.6: Passbands of the fourFLH532-10 filters from 512 nm to 552 nm nm.

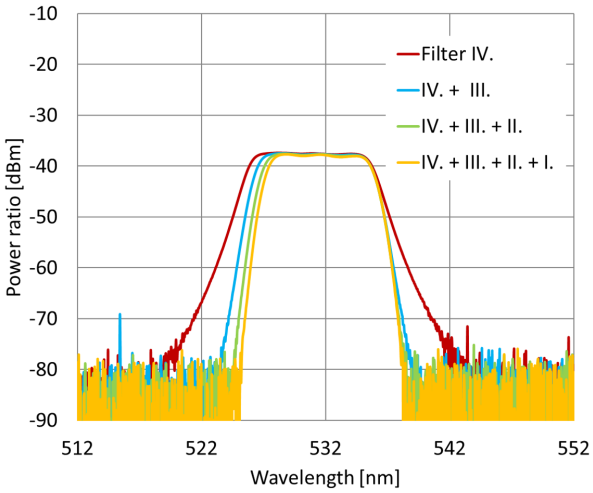

Figure 6.7: Edge Steepness of FLH532-10 filters measured from 512 nm to 552 nm, compared between one and a stack of two, three and four filters on a logarithmic scale.

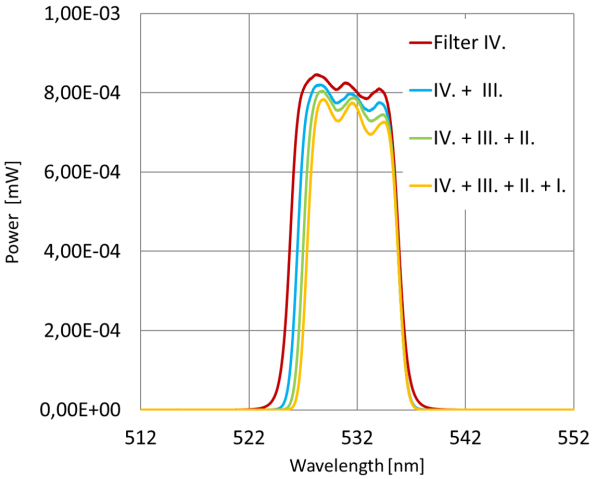

Figure 6.8: Edge Steepness of FLH532-10 filters measured from 512 nm to 552 nm, compared between one and a stack of two, three and four filters on a linear scale.

6.3 FBH660-10

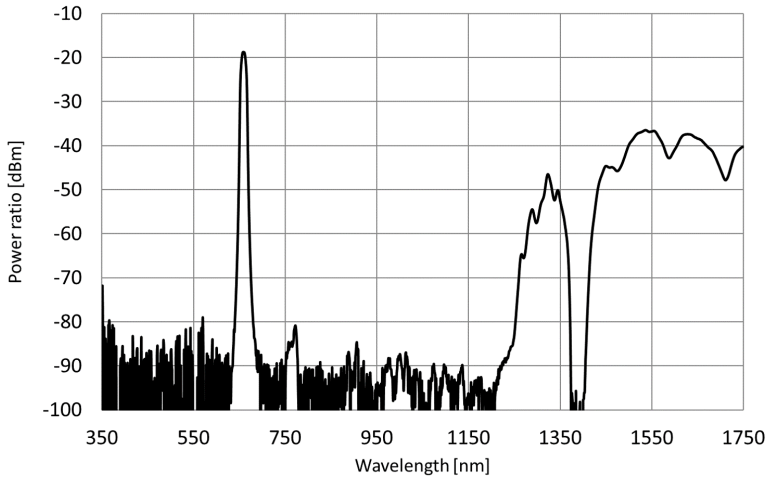

Figure 6.9: Spectrum of the FBH660-10 filter from 350 nm to 1750 nm.

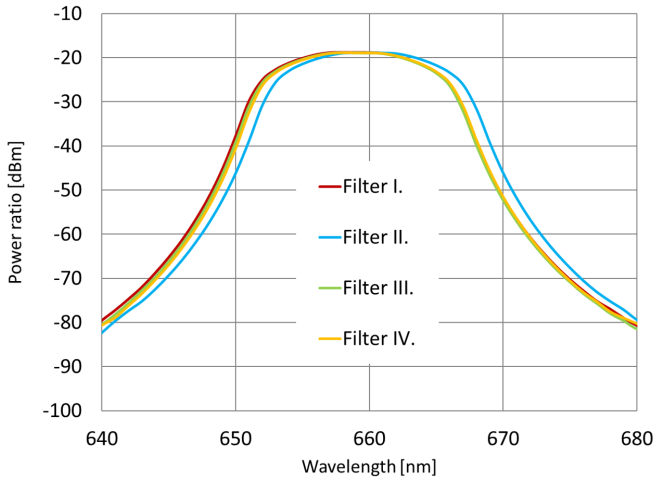

Figure 6.10: Passbands of the fourFBH660-10 filters from 640 nm to 680 nm.

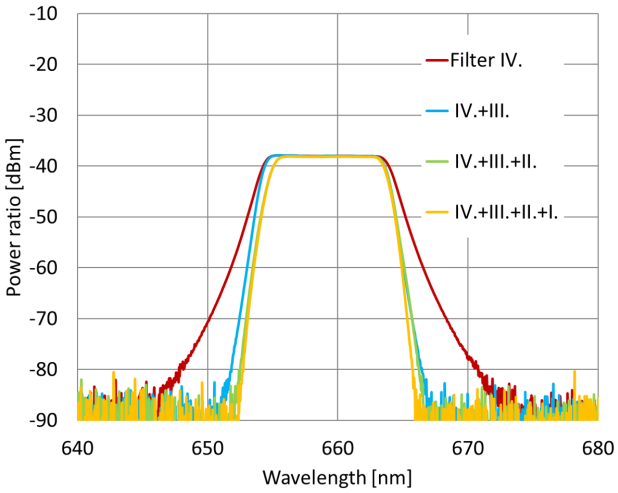

Figure 6.11: Edge Steepness of FBH660-10 filters measured from 640 nm to 680 nm, compared between one and a stack of two, three and four filters on a logarithmic scale.

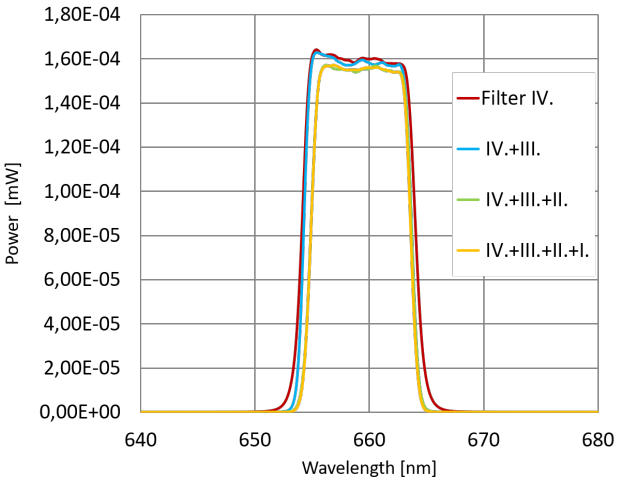

Figure 6.12: Edge Steepness of FBH660-10 filters measured from 640 nm to 680 nm, compared between one and a stack of two, three and four filters on a linear scale.

6.4 FBH780-10

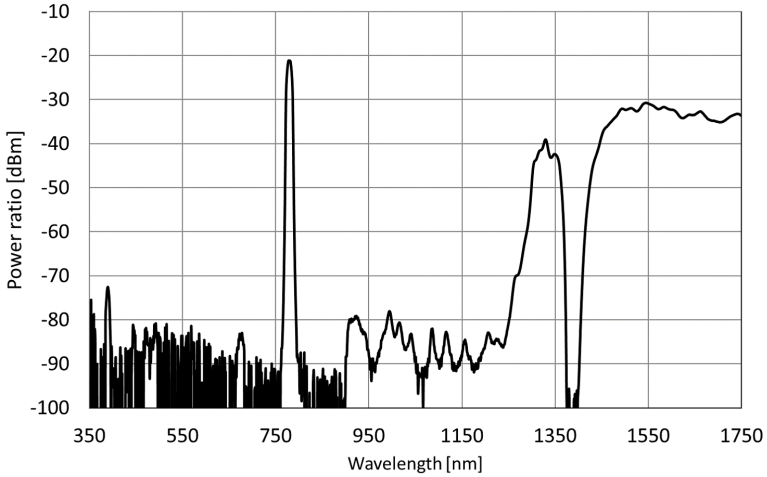

Figure 6.13: Spectrum of the FBH780-10 filter from 350 nm to 1750 nm.

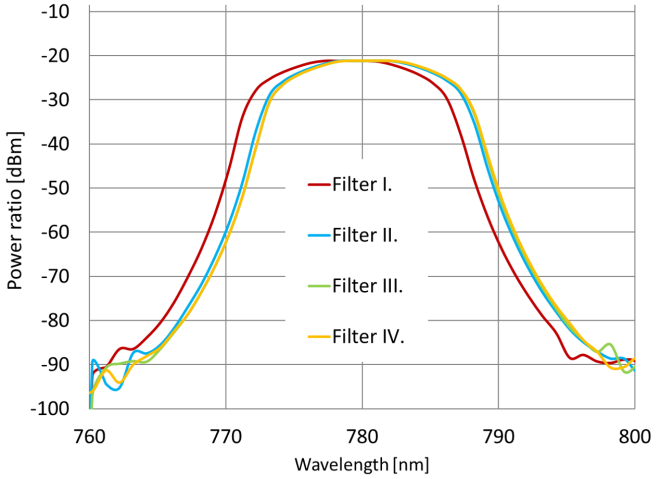

Figure 6.14: Passbands of the fourFBH780-10 filters from 760 nm to 800 nm.

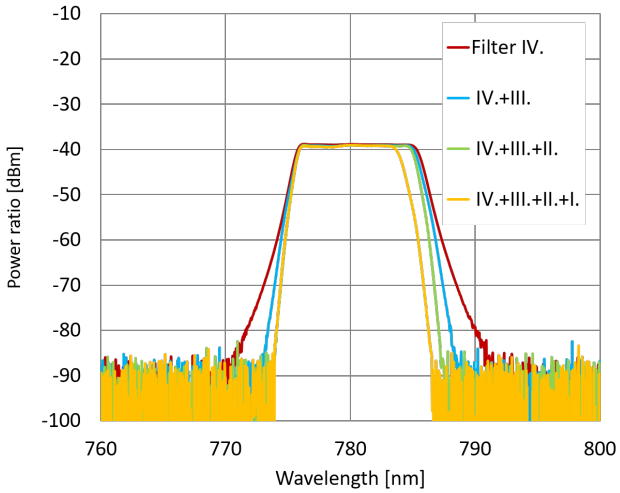

Figure 6.15: Edge Steepness of FBH780-10 filters measured from 760 nm to 800 nm , compared between one and a stack of two, three and four filters on a logarithmic scale.

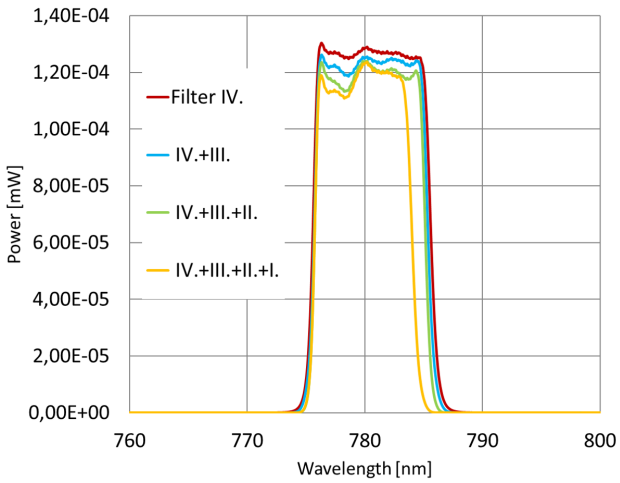

Figure 6.16: Edge Steepness of FBH780-10 filters measured from 760 nm to 800 nm, compared between one and a stack of two, three and four filters on a linear scale.

6.5 FBH850-10

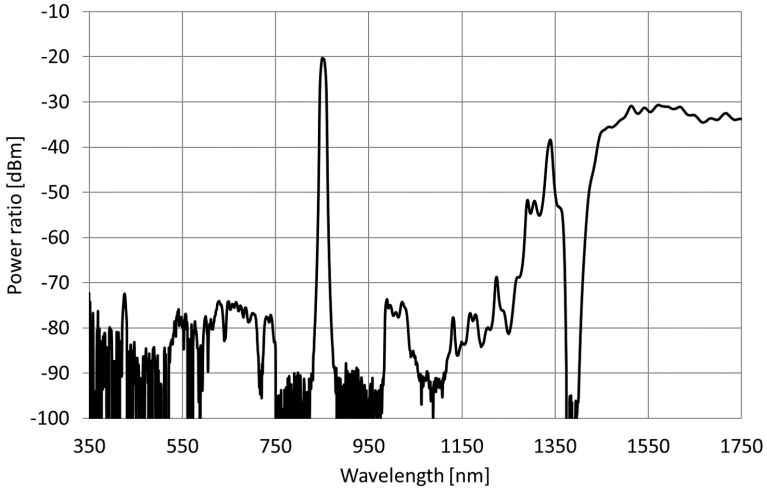

Figure 6.17: Spectrum of the FBH850-10 filter from 350 nm to 1750 nm.

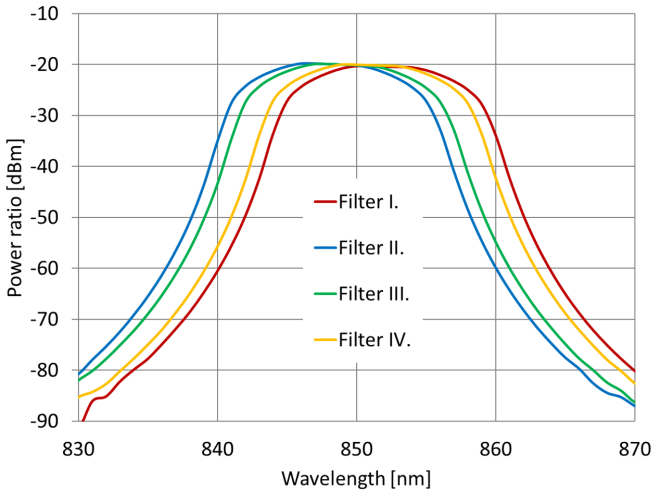

Figure 6.18: Passbands of the fourFBH850-10 filters from 830 nm to 870 nm.

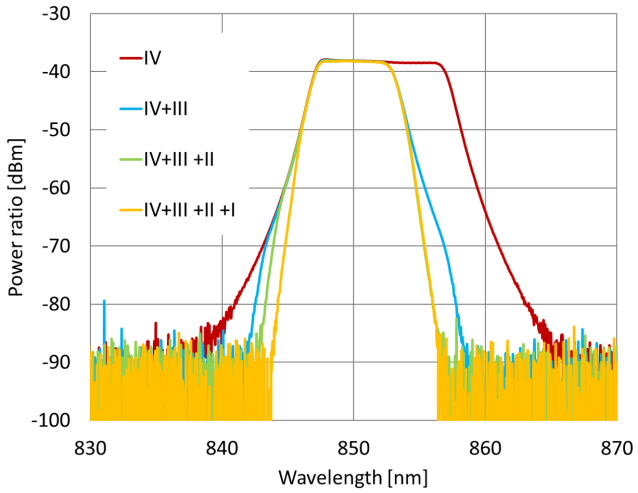

Figure 6.19: Edge Steepness of FBH850-10 filters measured from 830 nm to 870 nm , compared between one and a stack of two, three and four filters on a logarithmic scale.

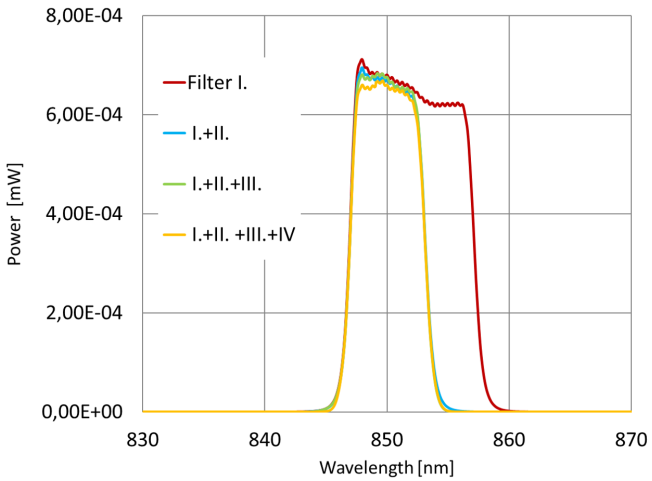

Figure 6.20: Edge Steepness of FBH850-10 filters measured from 830 nm to 870 nm, compared between one and a stack of two, three and four filters on a linear scale.

6.6 FB950-10

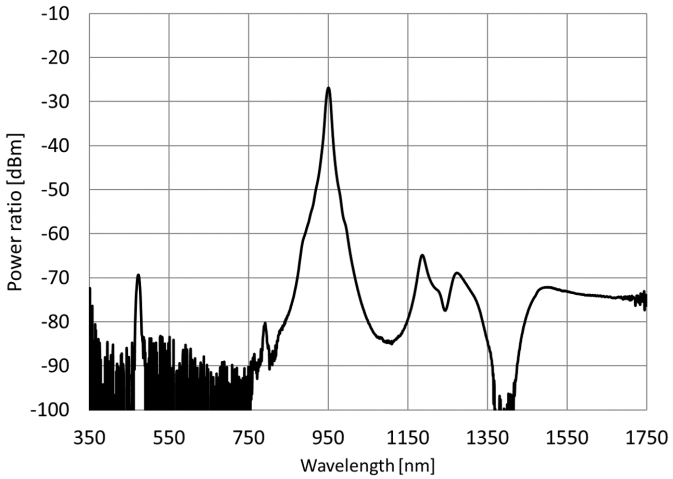

Figure 6.21: Spectrum of the FB950-10 filter from 350 nm to 1750 nm.

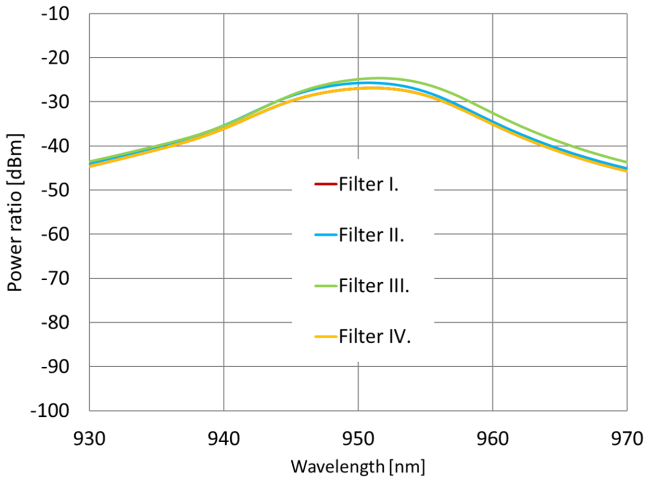

Figure 6.22: Passbands of the fourFB950-10 filters from 930 nm to 970 nm.

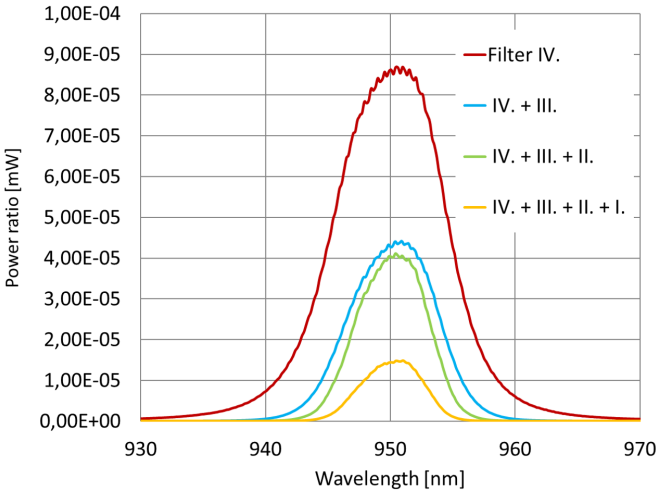

Figure 6.23: Edge Steepness of FB950-10 filters measured from 930 nm to 970 nm, compared between one and a stack of two, three and four filters on a linear scale.

References

[1] X. Baillard, A. Gauguet, S. Bize, P. Lemonde, Ph Laurent, A. Clairon, and P. Rosenbusch. Interference-filter-stabilized external-cavity diode lasers. *Optics Communications*, 266(2):609–613, 2006.

[2] Burak Bitlis. Parametric point spread function modeling and reduction of stray light effects in digital still cameras. *Computational Imaging V*, 6498(February 2007):1–8, 2007.

[3] M. Czerny and A. F. Turner. Ueber den Astigmatismus bei Spiegelspektrometern. *Zeitschrift fuer Physik*, 61(11-12):792–797, 1930.

[4] Hong Du and Kenneth J. Voss. Effects of Point-Spread Function on Calibration and Radiometric Accuracy of CCD Camera. *Applied Optics*, 43(3):665, 2004.

[5] Albert Einstein. Ueber die Entwicklung unserer Anschauungen ueber das Wesen und die Konstitution der Strahlung. *Physikalische Blätter*, 25(9):386–391, 1969.

[6] Energetiq Technology Inc. EQ-99XFC - Data Sheet.

[7] EnMAP Science Advisory Group. The EnMAP Space Mission, 2014.

[8] Christoph Gerhard. *Tutorium Optik*. 2016.

[9] Heinz Haferkorn. *Optik : physikalisch-technische Grundlagen und Anwendungen*. 4. edition, 2003.

[10] Eugene Hecht. *Optik*. 6. edition, 2014.

[11] James E Howard. Imaging properties of off-axis parabolic mirrors. *Applied Optics*, 18(15):2714, 1979.

[12] Robert P. Jansson, Peter A.; Breault. Correcting Color-Measurement Error Caused by Stray Light in Image Scanners. *Color and Imaging Conference, 6th Color and Imaging Conference Final Program and Proceedings*, pages 69–73, 1998.

[13] Karim Lenhard, Andreas Baumgartner, Peter Gege, Saulius Nevas, Stefan Nowy, and Armin Sperling. Impact of improved calibration of a NEO HySpex VNIR-1600 sensor on remote sensing of water depth. *IEEE Transactions on Geoscience and Remote Sensing*, 53(11):6085–6098, 2015.

[14] P. H. Lissberger. Properties of All-Dielectric Interference Filters. I. A New Method of Calculation. *Journal of the Optical Society of America*, 49(2):146–147, 1959.

[15] P. H. Lissberger and W. L. Wilcock. Properties of All-Dielectric Interference Filters. II. Filters in Parallel Beams of Light Incident Obliquely and in Convergent Beams. *Journal of the Optical Society of America*, 49(2):126–130, 1959.

[16] N.Bohr. Quantum Postulate and the Recent Development of Atomic Theory. *Nature*, pages 580–590, 1928.

[17] Thorlabs. Off-Axis Parabolic Mirrors, Protected Silver Coating (450 nm - 20 m).

[18] Gerd Wedler. *Lehrbuch der Physikalischen Chemie*. 4. edition, 1997.

[19] Yokogawa. AQ6370 Series Optical Spectrum Analyzer.

[20] Yuqin Zong, Steven W. Brown, B. Carol Johnson, Keith R. Lykke, and Yoshi Ohno. Simple spectral stray light correction method for array spectroradiometers. *Applied Optics*, 45(6):1111, 2006.